Stress inversion meets plasticity theory: A review of the theories of fault-slip analysis from the perspective of the deviatoric stress-strain space

Atsushi Yamaji[a], Katsushi Sato[a]

[a] Division of Earth and Planetary Sciences, Kyoto University, Kyoto 606-8502, Japan

Abstract

The mechanical behavior of materials is not affected by our choice of a coordinate system. Thus, the description of the behavior should not be affected by this choice. This is known as the principle of coordinate invariance, and is important not only for plasticity theory but for theoretical investigations in structural geology. The deviatoric stress-strain space, which fulfills the principle, is shown to be useful for the formulation of stress inversion. Problems in the inversion schemes of fault data are transformed into geometrical problems so that we can solve the problems using geometrical interpretations. In addition, the formulation gives the good basis for defining the classes of dissimilarities between reduced stress tensors that are the solutions of the inversion. We redefine the classes, here, from the standpoint of probability. It is demonstrated finally that the violation of the principle spoils the accuracy and resolution of the inversion.

Keywords: stress space, fault-slip analysis, paleostress, hyperspherical Lissajous

1. Introduction

Paleostresses themselves are unobservable, but are inferred from geologic structures, i.e., permanent deformations brought about beyond yield conditions. Thus, plasticity theory, which deals with stresses and permanent deformations, provides a clear perspective for the methodology of stress inversion of various geologic structures. The theories of plasticity has inspired structural geologists and seismologists to develop their methods to evaluate tectonic strains (e.g., Conel, 1962; Arthaud, 1969; Arthaud and Mattauer, 1969; Groshong, 1972; Mattauer, 1973; Kostrov, 1974; Hyndman and Weichert, 1983; Molnar, 1983; Gauthier and Angelier, 1985; Jackson and McKenzie, 1988; Marrett and Allmendinger, 1990; Cladouhos and Allmendinger, 1993) and stresses (e.g., Turner, 1953; Rebetsky, 1997, 1999; Fry, 1999, 2001; Sato and Yamaji, 2006a; Axen et al., 2015; Rebetsky et al., 2012; Matsumoto, 2016).

A researcher who conducts paleostress analysis expects that paleostress may be different from the present one, the deformation of which may have overprinted the deformation due to the paleostress. Consequently, the researcher is confronted with heterogeneous data, i.e, the collections of fault-slip data that may belong to different deformation events. However, the ages of the structures are usually debatable. Since the stress inversion of faults was proposed some 40 years ago (Carey and Brunier, 1974; Angelier, 1979), the heterogeneity has raised problems (e.g., Angelier and Manoussis, 1980).

However, the methodology to deal with heterogeneous fault-slip data has been greatly advanced in the last quarter century (Tikoff et al., 2013) by a number of researchers (e.g., Etchecopar et al., 1981; Gómez, 1986; Nemcok and Lisle, 1995; Nem-cok et al., 1999; Yamaji, 2000; Shan et al., 2003; Rocher et al., 2004; Yamaji et al., 2006; Tranos, 2015; Yamaji, 2015b; Parlangeau et al., 2018). The five-dimensional, deviatoric, stress-strain space of plasticity theory (Prager, 1949; Il'yushin, 1954; Payne, 1959) provides a clear formulation for the stress inversion to tackle this problem (Fry, 1999, 2001; Sato and Yamaji, 2006a). Il'yushin utilized this parameter space to deal with non-proportional loading, in which stress and strain orientations had temporal variation (Il'yushin, 1954, 1961; Wu, 2005, Chapter 7). So, the parameter space is suitable for coping with polyphase tectonics, which results in heterogeneous data sets for the stress inversion.

The strong point of inversion using the parameter space is that the inversion results are independent of the choice of a coordinate system in the physical space. The independence comes from the fact that the formulation takes into account the principle of coordinate invariance of plasticity theory, the principle states that material response is independent of the coordinate system we choose (e.g., Ottosen and Ristinmaa, 2005). This principle is trivially fulfilled when physical quantities and their relations are written in terms of tensors. Points in the deviatoric stress-strain space represent three-dimensional, symmetric, deviatoric tensors (Malvern, 1969; Khan and Huang, 1995; Ottosen and Ristinmaa, 2005).

The purpose of this paper is to summarize the theories of stress inversion of fault-slip data from the perspective using the deviatoric stress-strain space, and to provide mathematical apparatus for the researchers who study the stress inversion. The space is introduced, and problems concerning the inversion are addressed in §§2–5. The dissimilarity classes for inversion results are redefined in §6. Popular inversion schemes are reformulated using the space and reviewed in §7. It is demonstrated in §8 that the accuracy and resolution of the inversion is spoiled
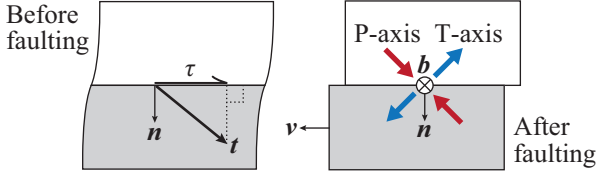
Figure 1: The direction of shear stress, τ, on a foot-wall before faulting is opposite to its displacement. t is the traction acting on the foot-wall before faulting. The P- and T-axes of a fault are coplanar with n and v, and are inclined at 45° from the fault plane.

by the violation of the principle. It is beyond the scope of this paper to review the applications of stress inversion to natural data or to detail the inverse methods based on other formulations. Reviews of this kind are those of Angelier (1994), Ramsay and Lisle (2000, Session 28), Lacombe (2010), Lacombe (2012), Célérier et al. (2012), Maury et al. (2013), Tikoff et al. (2013), Tavani et al. (2015) and Stephens et al. (2018).

2. Mathematical symbols

Vectors are denoted by column matrices throughout of this paper. Matrices and second-order tensors are denoted by bold symbols. Three-dimensional (3D) vectors are denoted by bold symbols, e.g., n, and 5D and 6D vectors are represented by arrows, e.g., $\vec{s}$ (Table 1). We identify vectors with the points that they indicate as position vectors. A matrix inner product is denoted by a colon, e.g., $A : B = \sum_{i,j=1}^{3} A_{ij}B_{ij}$. The diagonal matrix with the diagonal components, a, b and c, is denoted by $\mathrm{diag}(a, b, c)$.

We refer S_n to a unit hypersphere in nD space, meaning that the distance of any point on S_n is at unit distance from the center of the hypersphere in a nD space. Though an ordinary plane has two dimensions, hyperplanes in the following sections have higher dimensions. We specify the dimensions by a bracketed number such that a hyperplane [n] is defined by linearly independent n base vectors in an $(n + 1)$D or higher dimensional space, or defined by the perpendicularity with a vector in an $(n + 1)$D space. An ordinary plane is a hyperplane [2]. A great circle is the intersection of a sphere and a plane through the center of the sphere. Likewise, a great circle [m] is the intersection of S_n and a hyperplane [m] through the center of S_n, where $n > m$. An ordinary great circle on S_3 is a great circle [2]. A great circle arc [n] is a part of a great circle [n].

Compression and shortening are treated as positive stress and strain in this article. A deviatoric stress tensor is denoted by σ and ς, the later being normalized by its second basic invariant (§4.1), and is called reduced stress tensor. That is, σ is proportional to ς. The principal stresses satisfy $\sigma_3 \leq \sigma_2 \leq \sigma_1$ as usual. Accordingly, the corresponding eigenvalues of ς satisfy $\varsigma_3 \leq \varsigma_2 \leq \varsigma_1$. The stress ratio is defined as $\Phi \equiv (\sigma_2 - \sigma_3)/(\sigma_1 - \sigma_3)$. This is equivalent to $(\varsigma_2 - \varsigma_3)/(\varsigma_1 - \varsigma_3)$. The reduced stress tensor lacks information on stress magnitude, but bears the information of stress orientation and Φ.

A fault-slip datum obtained from a striated fault plane is represented by the paired unit vectors, n and v. The former is the unit normal to the plane with the inward direction for the footwall (Fig. 1); and the latter indicates the slip direction of the footwall block. In the case of a vertical fault, n is defined to point towards the southeastern or northeastern fault-block, and v indicates the movement direction of the block. In case of an E-W trending vertical fault, n points due south and v indicates the moving direction of the southern block. We refer also to the trio, n, v and $b = n \times v$, as the fault-slip datum. The unit normal, n, is perpendicular to v; and the three vectors make up an orthonormal system. Fault-slip data are represented by the pairs or trios.

3. Homogeneous and heterogeneous data sets

Fault-slip data are said to be heterogeneous in literature if they are taken from faults activated by temporarily or spatially different stress conditions. However, this definition about heterogeneity is inconvenient because the conditions themselves are unknowns to be determined. Accordingly, in this article we call data homogeneous if a state of stress explains all the data. Two or more stresses are required to explain heterogeneous data.

Thus, the classification of homogeneous and heterogeneous sets depends on how the term 'explain' is defined. To this end, we use the Wallace-Bott hypothesis (Wallace, 1951; Bott, 1959), which states that v is parallel to the shear stress acting on the plane. The misfit angle of this fault is the angle between v and the slip direction predicted by using this hypothesis under an assumed stress . If the misfit angles of all faults are smaller than a given threshold, e.g., 30°, the data from the faults are considered to be explained by a stress, and to be homogeneous. Otherwise, they are heterogeneous.

4. Formulation of fault-slip analysis using the deviatoric stress-strain space

4.1. Tensor-vector type transformation

Points in the deviatoric stress-strain space represent three-dimensional, symmetric, deviatoric stress and strain tensors. The tensors in the physical space are identified with the points through a tensor-vector type transformation as follows. Let X be a 3×3 symmetric matrix representing a deviatoric tensor ($X = X^T$ and trace $X = 0$). The second basic invariant of X is

$$X_{\mathrm{II}} \equiv \frac{1}{2}\left(X_{11}^2 + X_{22}^2 + X_{33}^2\right) + X_{23}^2 + X_{31}^2 + X_{12}^2. \quad (1)$$

We refer the Roman numeral, II, to the second basic invariant of a symmetric tensor, e.g., σ_{II}. Tensor components are affected by coordinate rotations, but the values of invariants are remain constant. If X is such a tensor that is normalized by its second basic invariant, the tensor can be written as

$$X = \frac{2}{\sqrt{3}} Q \, \mathrm{diag}(\cos \Lambda, \cos(\Lambda - 120°), \cos(\Lambda + 120°))Q^T, \quad (2)$$

where Q is the orthogonal matrix indicating the eigenvectors of X (Khan and Huang, 1995, Eq. 4.50). Angelier (1984) used a
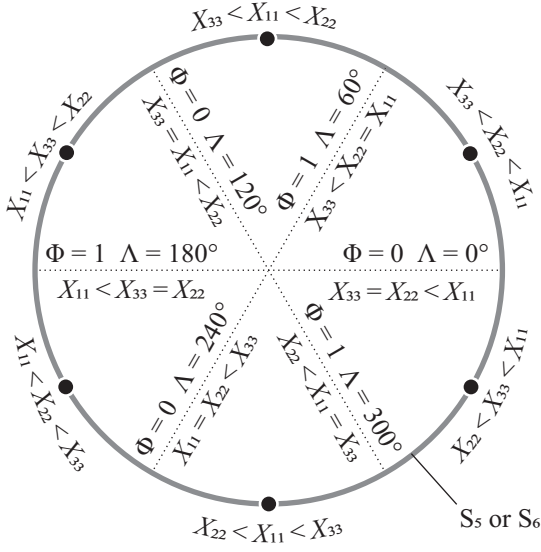
Figure 2: The correspondence of Λ and Φ. Inequalities of X_{11}, X_{22} and X_{33} hold true only for the case X has a diagonal form. Solid circles indicate the points where $\vec{h}$ and $\vec{p}$ can exist. See text in detail.

reduced stress tensor similar to Eq. (2). His tensor lacks the factor, $2/\sqrt{3}$. which makes X_{II} to be 1. Λ is called the Lode angle, and satisfies

$$\Phi = \frac{X_{\mathrm{int}} - X_{\mathrm{min}}}{X_{\mathrm{max}} - X_{\mathrm{min}}} = \frac{2\sin\Lambda}{\sqrt{3}\cos\Lambda + \sin\Lambda}, \tag{3}$$

for $0 \leq \Lambda \leq 60°$, where X_{min}, X_{int} and X_{max} are the minimum, intermediate and maximum eigenvalues of X, and

$$\Phi = \frac{2\sin(120° - \Lambda)}{\sqrt{3}\cos(120° - \Lambda) + \sin(120° - \Lambda)} \tag{4}$$

for $60° < \Lambda < 120°$. The graphs of the right-hand sides of Eqs. (3) and (4) have reflection symmetry with respect to the point, $\Lambda = 60°$. If Λ is in the interval, $[120°, 180°)$ or $[240°, 300°)$, Λ should be replaced with $(\Lambda \bmod 120°)$ in Eq. (3). If Λ is in the interval, $[180°, 240°)$ or $[300°, 360°)$, Λ is replaced with $(\Lambda \bmod 120°)$ in Eq. (4). As a result, Φ is a periodic function of Λ, and Φ is equal to $1/2$ (Fig. 2) when

$$\Lambda = 30°, \ 90°, \ 150°, \ 210°, \ 270° \ \text{or} \ 330°. \tag{5}$$

Φ is termed the shape ratio of X. In case where X stands for σ or ς, the shape ratio equals the stress ratio. So, we assign the symbol, Φ, to the shape ratio as well as the stress ratio. In the case where X stands for strain, the eigenvectors of X corresponding to X_{min} and X_{max} represent the orientations of the maximum shortening and maximum elongation, respectively. Thus, plane strain has the shape ratio at $1/2$. Strains with the ratio at 0 or 1 have oblate and prolate strain ellipsoids, respectively.

The symmetry of X allows us to identify X with the 6D vector,

$$\vec{X} = \left(\frac{X_{11}}{\sqrt{2}}, \frac{X_{22}}{\sqrt{2}}, \frac{X_{33}}{\sqrt{2}}, X_{23}, X_{31}, X_{12}\right)^{\mathrm{T}}. \tag{6}$$

That is, X can be obtained from $\vec{X}$, and vice versa. It follows from Eqs. (1) and (6) that $|\vec{X}| = \sqrt{X_{\mathrm{II}}}$. In the case of $X_{\mathrm{II}} = 1$, we have

$$|\vec{X}| = 1, \tag{7}$$

and $\vec{X}$ indicates a point on a unit hypersphere, S_6, in a 6D space. X and $\vec{X}$ carries the same information, and can be transformed from each other. Let X_1 and X_2 be symmetric, deviatoric tensors; and $\vec{X}_1$ and $\vec{X}_2$ be the corresponding 6D vectors. Then, we have

$$X_1 : X_2 = 2\vec{X}_1 \cdot \vec{X}_2. \tag{8}$$

The spaces that include these 6D vectors and the following 5D vectors are called the 6D and 5D deviatoric stress-strain spaces.

We can reduce the dimensionality of the vectors as follows (Fry, 1999). Analogous to the fact that a unit circle is the intersection of a unit sphere and a plane through its center, a unit hypersphere, S_5, in a 5D space is the intersection of S_6 and a hyperplane [5] through the center of S_6. The equation, trace $X = 0$, is equivalent with $\vec{P} \cdot \vec{X} = 0$, where $\vec{P} = (1, 1, 1, 0, 0, 0)^{\mathrm{T}}$. So, $\vec{X}$ is in the hyperplane [5] perpendicular to $\vec{P}$ through the center of S_6. Therefore, $\vec{X}$ is involved in the intersection of S_6 and the hyperplane [5]. That is, the intersection defines a unit hypersphere, S_5, in a 5D space. For this reason, the component of the vector, $\vec{X}$, along the $\vec{P}$-direction always vanishes, and can be truncated. So, $\vec{X}$ satisfies

$$R\vec{X} = \begin{pmatrix} 0 \\ \vec{Y} \end{pmatrix}, \tag{9}$$

where $\vec{Y}$ is a 5D vector, and R is a 6D rotation matrix that reorients the first coordinate axis to the $\vec{P}$ direction.

The components of R are determined from the linearly independent six vectors,

$$\begin{cases} \vec{P} \\ (0, 1, 0, 0, 0, 0)^{\mathrm{T}} \\ (0, 0, 1, 0, 0, 0)^{\mathrm{T}} \\ (0, 0, 0, 1, 0, 0)^{\mathrm{T}} \\ (0, 0, 0, 0, 1, 0)^{\mathrm{T}} \\ (0, 0, 0, 0, 0, 1)^{\mathrm{T}}. \end{cases} \tag{10}$$

From these vectors, the Gram-Schmidt process (e.g., Meyer, 2000) yields the orthonormal basis of the 6D space,

$$\begin{cases} \vec{P}/\sqrt{3} \\ (-1, 2, -1, 0, 0, 0)^{\mathrm{T}}/\sqrt{6} \\ (-1, 0, 1, 0, 0, 0)^{\mathrm{T}}/\sqrt{2} \\ (0, 0, 0, 1, 0, 0)^{\mathrm{T}} \\ (0, 0, 0, 0, 1, 0)^{\mathrm{T}} \\ (0, 0, 0, 0, 0, 1)^{\mathrm{T}}. \end{cases}$$

The components of the second through to the sixth vectors make up

$$R = \begin{pmatrix} \frac{1}{\sqrt{3}} & \frac{1}{\sqrt{3}} & \frac{1}{\sqrt{3}} & 0 & 0 & 0 \\ -\frac{1}{\sqrt{6}} & \frac{2}{\sqrt{6}} & -\frac{1}{\sqrt{6}} & 0 & 0 & 0 \\ -\frac{1}{\sqrt{2}} & 0 & \frac{1}{\sqrt{2}} & 0 & 0 & 0 \\ 0 & 0 & 0 & 1 & 0 & 0 \\ 0 & 0 & 0 & 0 & 1 & 0 \\ 0 & 0 & 0 & 0 & 0 & 1 \end{pmatrix}. \tag{11}$$

3

Since the choice of the second through sixth vectors in Eq. (10) is arbitrary, previous authors obtained somewhat different rotation matrices (Sato and Yamaji, 2006a; Yamaji, 2015a), but their formulations have a common physical meaning. The non-uniqueness is explained, e.g., by Wu (2005, p. 352).

X, $\vec{X}$ and $\vec{Y}$ have different mathematical expressions, but represent the same physical entity. Combining Eqs. (6), (9) and (11), we have

$$\vec{Y} = \left(-\frac{\sqrt{3}}{6}(X_{11} - 2X_{22} + X_{33}), \frac{-X_{11} + X_{33}}{2}, X_{23}, X_{31}, X_{12} \right)^{\mathrm{T}}.$$

The traceless condition, trace $X = 0$, simplifies the first component,

$$\vec{Y} = \left(-\frac{\sqrt{3}X_{22}}{2}, \frac{-X_{11} + X_{33}}{2}, X_{23}, X_{31}, X_{12} \right)^{\mathrm{T}}, \quad (12)$$

which describes the tensor-vector type transformation. On the other hand, X is obtained from $\vec{Y}$ using the inverse of Eq. (9):

$$\vec{X} = \mathbf{R}^{-1} \begin{pmatrix} 0 \\ \vec{Y} \end{pmatrix}. \quad (13)$$

Combining Eqs. (6), (11) and (13), we obtain

$$X = \begin{pmatrix} -\frac{1}{\sqrt{3}}Y_1 - Y_2 & Y_5 & Y_4 \\ Y_5 & \frac{2}{\sqrt{3}}Y_1 & Y_3 \\ Y_4 & Y_3 & -\frac{1}{\sqrt{3}}Y_1 + Y_2 \end{pmatrix}, \quad (14)$$

where Y_i is the ith component of $\vec{Y}$. Eq. (14) describes the vector-tensor type transformation.

4.2. Reduced stress and strain tensors and the Wallace-Bott hypothesis

Our reduced stress tensor satisfies trace $\varsigma = 0$ and $\varsigma_{\mathrm{II}} = 1$; and has the form,

$$\varsigma = \frac{1}{3\lambda} \mathbf{Q} \, \mathrm{diag}(2 - \Phi, 2\Phi - 1, -\Phi - 1) \mathbf{Q}^{\mathrm{T}}, \quad (15)$$

where

$$\lambda = \sqrt{(\Phi^2 - \Phi + 1)/3}. \quad (16)$$

In the case where the stress axes are parallel to the coordinate axes, Eq. (15) reduces to $\varsigma = \mathrm{diag}(\varsigma_1, \varsigma_2, \varsigma_3)$. Eq. (15) is equivalent with Eq. (2), but has Φ explicitly. The parameter, λ, simplifies the mathematical expressions involving differential stress (Yamaji, 2015a). We call this axiality because λ has the maximum, $1/\sqrt{3} \approx 0.58$ when the stress has axial symmetry ($\Phi = 0$ or 1): The minimum value of λ is 1/2 when $\Phi = 1/2$.

The paired reduced strain tensors, ϵ and ϵ', represent a fault-slip datum. $\mathbf{n}$, $\mathbf{v}$ and $\mathbf{b}$. That is, the tensors are defined to have the ijth components,

$$\epsilon_{ij} = -(v_i n_j + v_j n_i) \quad (17)$$
$$\epsilon'_{ij} = -(b_i n_j + b_j n_i). \quad (18)$$

Obviously, these are symmetric tensors ($\epsilon_{ij} = \epsilon_{ji}$ and $\epsilon'_{ij} = \epsilon'_{ji}$). The tensor with the ijth component, $v_i n_j$, or its symmetric part, $(v_i n_j + v_j n_i)/2$, is called Schmid tensor in plasticity theory (e.g., Kocks et al., 1998). The minus signs of Eqs. (17) and (18) mean that a shortening is a positive strain. The tensors in those equations represent simple shear along the $\mathbf{v}$ and $\mathbf{b}$ directions, respectively (Fig. 1). The tensors lack information about strain magnitudes, but bears information about strain orientations. The tensors can be defined for a twin datum as well.

The reduced strain tensors satisfy the equations of X in the last subsection because they satisfy

$$\mathrm{trace}\, \epsilon = \mathrm{trace}\, \epsilon' = 0, \quad \epsilon_{\mathrm{II}} = \epsilon'_{\mathrm{II}} = 1. \quad (19)$$

In addition, they also satisfy

$$\epsilon : \epsilon' = 0. \quad (20)$$

These tensor relations can be proven using the fault-slip datum (Fig. 3),

$$\mathbf{n} = (0, 0, -1)^{\mathrm{T}}, \quad \mathbf{v} = (-1, 0, 0)^{\mathrm{T}}, \quad \mathbf{b} = (0, 1, 0)^{\mathrm{T}}. \quad (21)$$

That is, these vectors have the corresponding tensors,

$$\epsilon = \begin{pmatrix} 0 & 0 & -1 \\ 0 & 0 & 0 \\ -1 & 0 & 0 \end{pmatrix}, \quad \epsilon' = \begin{pmatrix} 0 & 0 & 0 \\ 0 & 0 & 1 \\ 0 & 1 & 0 \end{pmatrix}. \quad (22)$$

Indeed, these tensors satisfy Eqs. (19) and (20). Note that we have not specified the directions of the coordinate axes to write the vector components in Eq. (21). Rectangular Cartesian coordinates can be arbitrarily oriented, and the vectors in Eq. (21) can point to any directions in the physical space. Hence, any fault-slip datum satisfies Eq. (19) as long as the datum is denoted by the orthonormal vectors, $\mathbf{n}$, $\mathbf{v}$ and $\mathbf{b}$. These vectors are first rank tensors, whereas ϵ and ϵ' are second rank ones. It is the advantage of describing physical quantities in terms of tensors that tensor relations are independent of the choice of a coordinate system (e.g., Aris, 1989). So it does for the tensor relations in Eq. (19) and (20).

The tensors in Eq. (22) have the eigenvalues, 0 and ±1, meaning that the tensors represent plane strains. The eigenvectors of ϵ are denoted by $\pm\mathbf{e}_{+1}$, $\pm\mathbf{e}_0$ and $\pm\mathbf{e}_{-1}$ in Fig. 3; and those of ϵ' by $\pm\mathbf{e}'_{+1}$, $\pm\mathbf{e}'_0$ and $\pm\mathbf{e}'_{-1}$. The subscripts denote the eigenvectors. The eigenvectors of a tensor are generally bidirectional: If $\mathbf{e}$ is an eigenvector of the tensor, $-\mathbf{e}$ is also en eigenvector. Accordingly, plus-minus signs are attached to emphasize the bidirectional character. $\pm\mathbf{e}_0$ and $\pm\mathbf{e}'_0$ are parallel to $\mathbf{b}$; and $\mathbf{v}$, respectively. $\pm\mathbf{e}_{+1}$ and. $\pm\mathbf{e}_{-1}$ meet $\mathbf{n}$ and $\mathbf{v}$ at the angles of 45°. So, they coincide with the P- and T-axes (Fig. 1). $\pm\mathbf{e}'_{+1}$ and $\pm\mathbf{e}'_{-1}$ meet $\mathbf{n}$ and $\mathbf{b}$ also at the angles of 45°. Note that the directions the Cartesian coordinates were not specified to define the vectors in Eq. (21). So, the orientations of the eigenvectors relative to the vectors in Fig. 3 are not affected by the choice of the coordinate directions.

The Wallace-Bott hypothesis, the basis of the majority of inversion schemes for faults and seismic focal mechanisms, is expressed as tensor relations as follows. Traction upon the fault
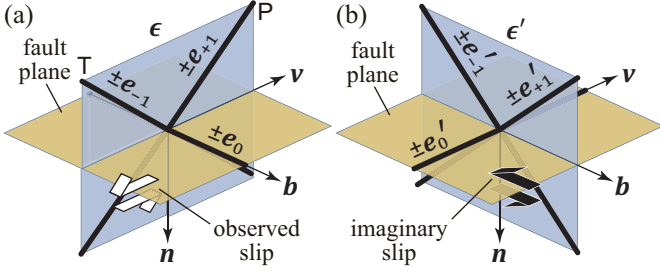
4

Figure 3: A fault-slip datum, n, v and $b = n \times v$ (Fig. 1), and the principal orientations (bold lines) of the corresponding strain tensors, ϵ and ϵ', both of which have the eigenvalues, $+1$, 0 and -1. The orientations parallel to the eigenvectors of ϵ are denoted by e_{+1}, e_0 and e_{-1}, where the subscripts indicate the corresponding eigenvalues. Likewise, those of ϵ' are indicated by e'_{+1}, e'_0 and e'_{-1}. The imaginary slip along b direction, which brings about the imaginary strain ϵ', is shown in (b).
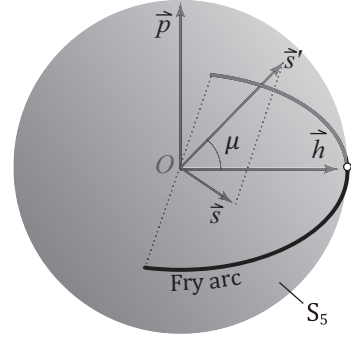

Figure 4: Schematic illustrations of Fry arcs (thick lines) on S_5. The orthogonal projection of $\vec{s}$ onto the plane spanned by $\vec{h}$ and $\vec{p}$ is denoted by $\vec{s}''$. The line through the ends of the arc is depicted by a dotted line. Open circle indicates the center of the arc denoted by $\vec{h}$. Shear stress on the fault corresponding to the arc has the maximum value when $\vec{s}$ indicate this point.

Figure 5:

is denoted by $t = \varsigma n$. The direction of shear stress must be opposite to v (Fig. 1). Therefore, we have $v \cdot t < 0$. It follows that $v \cdot \varsigma n = \sum_{i,j=1}^3 \varsigma_{ij} v_i n_j = \sum_{i,j=1}^3 \varsigma_{ij} (v_i n_j + v_j n_i)/2 = (\varsigma : \epsilon)/2 < 0$, where Eq. (18) and the symmetry, $\epsilon_{ij} = \epsilon_{ji}$, are used. On the other hand, the Wallace-Bott hypothesis is expressed as $b \cdot t = 0$ (Angelier and Goguel, 1979), which is rewritten as $\sum_{i,j=1}^3 \varsigma_{ij} b_i n_j = (\varsigma : \epsilon')/2 = 0$. Thus, faulting satisfies the inequality and equation,

$$\varsigma : \epsilon > 0, \quad \varsigma : \epsilon' = 0. \tag{23}$$

This inequality states that the energy dissipation by faulting must be positive in sign (Yamaji and Sato, 2006). It means that the inequality always holds irrespective of the hypothesis.

4.3. 5D and 6D vectors representing stresses and fault-slip data

Not only the reduced stress tensor, but also the reduced strain tensors are expressed as 6D unit vectors (Eqs. 6 and 7). That is, the vectors,

$$\begin{cases} \vec{\varsigma} = \left(\dfrac{\varsigma_{11}}{\sqrt{2}}, \dfrac{\varsigma_{22}}{\sqrt{2}}, \dfrac{\varsigma_{33}}{\sqrt{2}}, \varsigma_{23}, \varsigma_{31}, \varsigma_{12} \right)^{\mathrm{T}} \\ \vec{\epsilon} = -\left(\sqrt{2} n_1 v_1, \sqrt{2} n_2 v_2, \sqrt{2} n_3 v_3, \right. \\ \qquad\qquad \left. n_2 v_3 + n_3 v_2, n_3 v_1 + n_1 v_3, n_1 v_2 + n_2 v_1 \right)^{\mathrm{T}} \\ \vec{\epsilon}' = -\left(\sqrt{2} n_1 b_1, \sqrt{2} n_2 b_2, \sqrt{2} n_3 b_3, \right. \\ \qquad\qquad \left. n_2 b_3 + n_3 b_2, n_3 b_1 + n_1 b_3, n_1 b_2 + n_2 b_1 \right)^{\mathrm{T}}. \end{cases} \tag{24}$$

represent stress and a datum from a fault or a mechanical twin. It follows from (Eq. 20) that $\vec{\epsilon} \cdot \vec{\epsilon}' = 0$, i.e., $\vec{\epsilon}$ and $\vec{\epsilon}'$ are perpendicular to each other.

Now, Eq. (8) allows us to rewrite the conditions in Eq. (23) as the pair, $\vec{\varsigma} \cdot \vec{\epsilon} > 0$ and $\vec{\varsigma} \cdot \vec{\epsilon}' = 0$. This pair means that $\vec{\varsigma}$ is perpendicular to $\vec{\epsilon}'$ and makes an acute angle with $\vec{\epsilon}$, i.e., they state that the endpoint of $\vec{\varsigma}$ exists on the great-circle arc [4] with the pole, $\vec{\epsilon}'$ and the arc length of $180°$ centered by $\vec{\epsilon}$. We call it a 6D Fry arc. We can reduce the dimensionality of the arc using Eq. (9). That is, the geometrical propositions concerning $\vec{\varsigma}$, $\vec{\epsilon}$

and $\vec{\epsilon}'$ hold for the corresponding 5D vectors. As a result, we obtain the 5D vectors,

$$\vec{s} = \left(\dfrac{\sqrt{3}}{2} \varsigma_{22}, \dfrac{1}{2}(-\varsigma_{11} + \varsigma_{33}), \varsigma_{23}, \varsigma_{31}, \varsigma_{12} \right)^{\mathrm{T}}$$

$$\vec{h} = \left(\sqrt{3} n_2 v_2, -n_1 v_1 + n_3 v_3, \right.$$
$$\qquad\qquad \left. n_2 v_3 + n_3 v_2, n_3 v_1 + n_1 v_3, n_1 v_2 + n_2 v_1 \right)^{\mathrm{T}}$$

$$\vec{p} = \left(\sqrt{3} n_2 b_2, -n_1 b_1 + n_3 b_3, \right.$$
$$\qquad\qquad \left. n_2 b_3 + n_3 b_2, n_3 b_1 + n_1 b_3, n_1 b_2 + n_2 b_1 \right)^{\mathrm{T}}, \tag{25}$$

where 's,' 'h' and 'p' stand for stress, hemisphere and pole. Inheriting the properties of the 6D vectors, these vectors satisfy

$$|\vec{s}| = |\vec{h}| = |\vec{p}| = 1, \quad \vec{h} \cdot \vec{p} = 0. \tag{26}$$

4.4. 5D Fry arc

By means of the 5D vectors, the condition of faulting is written as

$$\vec{p} \cdot \vec{s} = 0, \quad \vec{h} \cdot \vec{s} > 0. \tag{27}$$

A 5D Fry arc on S_5 is defined by the pair in (27) (Fig. 5). That is, $\vec{s}$ is involved in the equatorial hyperplane [4] with the pole, $\vec{p}$, and is in the hemisphere centered by $\vec{h}$. The components of $\vec{s}$, $\vec{h}$ and $\vec{p}$ are affected by the choice of a coordinate system in the physical space, but Eqs. (26) and (27) hold irrespective of the choice. Thus, the formulation of stress inversion using the vectors acquires the coordinate invariance.

The point indicated by $\vec{s}$ can exist anywhere on S_5, but those indicated by $\vec{h}$ or $\vec{p}$ are not. Note that S_5 is a curved 4D space, analogous to a sphere in the physical space is a curved 2D space. In contrast, a fault-slip datum denoted by n, v and b has only three-degrees of freedom, which is represented by, for example, the dip and strike of the fault plane and the rake of the
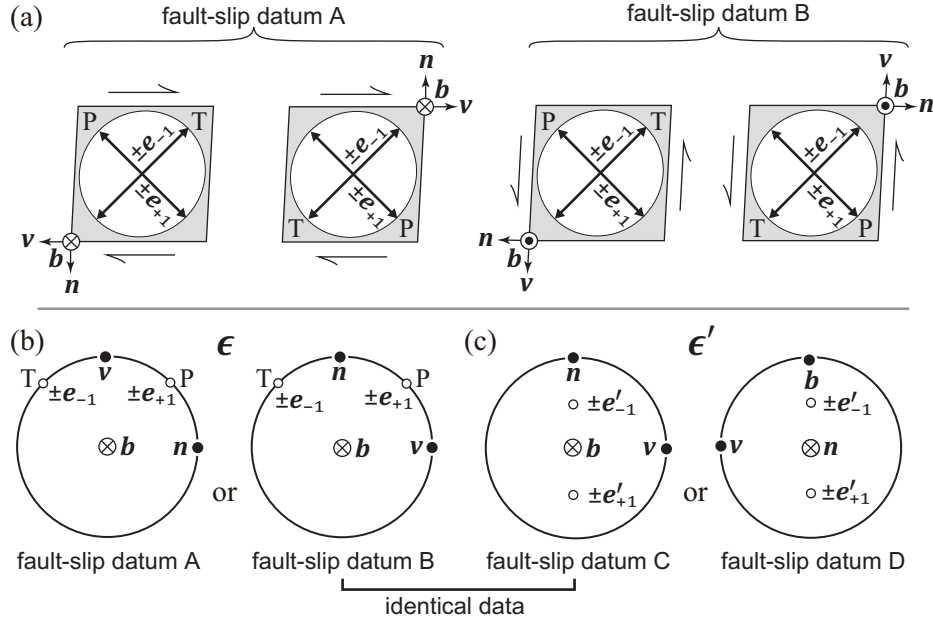
5

Figure 6: (a) Four possible directions of n, v and b compatible with a strain tensor, ϵ. The first two possibilities indicate the fault movements of footwall and hangingwall block, and are geologically identical. This is called the fault-slip datum A. The latter two among the four possibilities are also geologically identical, and indicate the fault-slip datum B. (b) Stereoplot of the fault-slip data A and B compatible with ϵ. (c) Stereoplot of the fault-slip data C and D compatible with ϵ'. A Fry arc is represented by ϵ and ϵ'. P and T denote the P- an T-axes for the faults represented by n, v and b.

slip direction. Accordingly, the pair, $\vec{h}$ and $\vec{p}$, has only three-degrees of freedom. Consequently, neither $\vec{h}$ nor $\vec{p}$ densely covers S_5. The eigenvalues of both ϵ and ϵ' are 0 and ± 1. X has the same eigenvalues only when Λ has a value of Eq. (5). Otherwise, ϵ and ϵ' do not indicate plane strains. Therefore, the points on S_5 indicated by any $\vec{h}$ or $\vec{p}$ must have the shape ratio at 1/2. Other points on S_5 cannot have corresponding fault-slip data.

4.5. Mapping from a 5D Fry arc to a fault-slip datum

A fault-slip datum denoted by the trio, n, v and b, has a one-to-one correspondence with a Fry arc. It has been shown above that a Fry arc is uniquely determined from a datum. The opposite is shown below using an example. Suppose that a Fry arc with $\vec{h} = (0, 0, 0, 1, 0)^T$ and $\vec{p} = (0, 0, -1, 0, 0)^T$ is given. These vectors are transformed through Eq. (14) to the reduced strain tensors. The results are shown in Eq. (22) which have the eigenvalues +1, 0 and -1. The principal orientations of ϵ corresponding to the eigenvalues, +1 and -1, are parallel to the P- and T-axes, respetively. However, there are four trios of n, v and b that have the eigenvectors in common (Fig. 6). How do we choose the trio appropriate to the Fry arc?

The appropriate trio is chosen as follows. Let e_{+1}, e_0, e_{-1} be the eigenvectors of ϵ; and e'_{+1}, e'_0, e'_{-1} be those of ϵ' of ϵ'. The subscripts indicate the corresponding eigenvalues. The angular relations of these eigenvectors and the trio, n, v and b, are shown in Fig. 3. The orientations of b are readily given as $b = \pm e_0$, and those of n and v as the bisectors of $\pm e_{+1}$ and $\pm e_{-1}$. However, the directions of n, v and b remain uncertain due to the fact that the eigenvectors are bidirectional. As a result, ϵ

gives four possible trios (Fig. 6a) and two possible fault-slip data (Fig. 6b). Likewise, ϵ' gives two possible fault-slip datum (Fig. 6c). Finally, we can choose uniquely the fault-slip datum corresponding to the given Fry arc by finding the identical fault-slip datum in Figs. 6b and c. Thanks to the coordinate invariance of the present formulation, this procedure is good for any Fry arc to determine the corresponding fault-slip datum. Note that the pair, n and v, cannot be determined uniquely only from h, nor from ϵ.

4.6. Some important properties of the deviatoric stress-strain space

Important quantities of stress inversion can be interpreted as geometrical relations in the 5D space. For example, antipodal points on S_5 indicate the opposite stresses, under which faults slip in the opposite directions irrespective of their attitudes (Fry, 1999). That is, given a state of stress with the stress ratio, Φ, its opposite stress is obtained by interchanging the σ_1- and σ_3-axes and exchanging Φ with $1 - \Phi$. Orife and Lisle (2003) called the second tensor the negative tensor of the first one. The misfit angle, μ, between v and the theoretical slip direction for ς is equal to the angle between $\vec{h}$ and the orthogonal projection of $\vec{s}$ onto the plane spanned by $\vec{h}$ and $\vec{p}$ (Fig. 5) (Sato and Yamaji, 2006a).

Given two reduced stress tensors, a reduced stress tensor between them can be obtained through the following procedure. Let $\vec{s}^{(1)}$ and $\vec{s}^{(2)}$ be the points on S_5 corresponding to the two tensors. Then, their intermediate tensor is represented by the

6

point,

$$\vec{s} = \left[\frac{\sin(t\Theta)}{\sin\Theta} \right] \vec{s}^{(1)} + \left\{ \frac{\sin[(1-t)\Theta]}{\sin\Theta} \right\} \vec{s}^{(2)}, \qquad (28)$$

where Θ is the angle between $\vec{s}^{(1)}$ and $\vec{s}^{(2)}$, and $0 \le t \le 1$. This is the spherical linear interpolation (e.g., Ghali, 2008) of points along S_5. The point, $\vec{s}$, moves with increasing t along the great circle [2] from $\vec{s}^{(1)}$ to $\vec{s}^{(2)}$.

Stress magnitude can be incorporated into the 5D space as follows (Yamaji, 2015a). That is, deviatoric stress tensor has the expression, $\boldsymbol{\sigma} = \lambda\Delta\sigma\boldsymbol{\varsigma}$, where λ is defined in Eq. (16), and $\Delta\sigma$ is differential stress. This tensor corresponds to the vector, $\lambda\Delta\sigma\vec{s}$, in the 5D deviatoric stress-strain space. The resolved shear stress along $\boldsymbol{v}$ in the physical space is written as

$$\tau = \lambda\Delta\sigma\vec{s} \cdot \vec{h}. \qquad (29)$$

Deviatoric stress tensor, $\lambda\Delta\sigma\boldsymbol{\varsigma}$, has a one-to-one correspondence with the 5D vector, $\lambda\Delta\sigma\vec{s}$.

It follows that τ has the maximum value if $\vec{s}$ is at the center of the Fry arc (Fig. 5). In this case, the fault is the most favorably oriented fault under the state of stress denoted by s, and its P- or T-axes (when $\Phi = 0$ or 1) or both (when $0 < \Phi < 1$) are parallel to the σ_1- and σ_3-axes, respectively. In contrast, τ vanishes at the ends of a Fry arc even for $\Delta\sigma > 0$. Note that the ends of a Fry arc represent 3D subspace (i.e., a hyperplane [3]) in the 5D deviatoric stress-strain space, because the ends are defined by the set of position vectors perpendicular to the 2D plane spanned by $\vec{h}$ and $\vec{p}$. When a fault plane is parallel to a stress axis in the physical space, $\vec{s}$ is in the 3D subspace perpendicular to this 2D plane; and the resolved shear stress vanishes on the fault plane.

Eq. (29) shows the factorization of the resolved shear stress into the factors of axiality, differential stress, s- and h-vectors. This expression is useful for the stress inversion of mechanical twin data (Yamaji, 2015a,b). Transforming the s-vector into the corresponding reduced stress tensor, we have another expression for the factorization of resolved shear stress: $\tau = -\lambda\Delta\sigma\boldsymbol{v}\boldsymbol{\varsigma}\boldsymbol{n}$ (Yamaji, 2015a, Eq. 11). The minus sign comes from the opposite directions of $\boldsymbol{v}$ and shear stress (Fig. 1).

5. Trajectories on S_5

The resolution and accuracy of stress inversion is concerned with the temporal and/or spatial perturbation of reduced stress tensor and with the perturbations due to measurement errors. The perturbation makes the point, $\vec{s}$, migrate on S_5; and the perturbations due to the errors result in the shifting of the points denoted by h- and p-vectors. Thus, it is essential to understand how the perturbations in the physical space lead to the migration of the points on S_5. So, we investigated the trajectories of the point, $\vec{Y}$, on S_5 corresponding to the rotation of the principal axes of X and to a change in Λ (Eq. 2). Since the mathematical equations and their derivation processes of the trajectories are lengthy, they are shown in the Supplement.
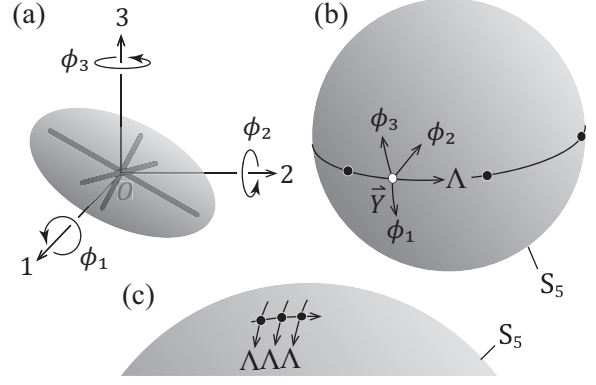

Figure 7: (a) Rotations about the axes of rectangular Cartesian coordinates. Thick lines depict the principal axes of the gray ellipsoid that visualizes the symmetric matrix X. (b) Schematic illustration of the trajectories of the endpoint of $\vec{Y}$ on S_5 defined by the change of either of the values of Λ, ϕ_1, ϕ_2 or ϕ_3. Solid circles indicate the points on S_5 where $\vec{h}$ and $\vec{p}$ can exist. The points are arranged with 60° intervals along the Λ direction. (c) The continuous movement of a datum point (solid circles) and the trajectory, $\vec{Y}(\Lambda)$, associated with successive rotations about a fixed axis in the physical space.

5.1. Lode angle

The position of the point, $\vec{Y}$, on S_5 is a function of the principal orientations (Fig. 7a) and the shape ratio of X in the physical space (Eq. 2). The orientations are denoted by $\boldsymbol{Q}$. When $\boldsymbol{Q}$ is kept constant, the trajectory on S_5 has only the parameter, Λ, which denotes the shape ratio. That is, we have the function, $\vec{Y}(\Lambda)$. As a result, $\vec{Y}(\Lambda)$ is a great circle [2] on S_5 (Fig. 7b). This is shown as follows. Eq. (2) and the trigonometric identity, $\cos(\Lambda \pm 2\pi/3) = -(1/2)\cos\Lambda \mp (\sqrt{3}/2)\sin\Lambda$, allow us to rewrite the components of X in Eq. (2) in terms of the linear combinations of $\sin\Lambda$ and $\cos\Lambda$. The same is true for the components of $\vec{Y}$ in Eq. (12), such that $\vec{Y}$ has the ith component, $A_i\sin\Lambda + B_i\cos\Lambda$. The coefficients, A_i and B_i are the linear combinations of the quadratic terms of the components of $\boldsymbol{Q}$. Since the point, $\vec{Y}$, is constrained upon S_5, the 5D vector with the ith component,

$$T_i \equiv \frac{\partial Y_i}{\partial\Lambda} = A_i\cos\Lambda - B_i\sin\Lambda, \qquad (30)$$

is tangent to the trajectory, $\vec{Y}(\Lambda)$ (e.g., Lipschutz et al., 2009). It can be seen that $|\vec{T}| = 1$ (Supplement). Then, the 5D vector, $\vec{K} \equiv \partial\vec{T}/\partial\Lambda$, indicates the local curvature of the trajectory. $\vec{K}$ generally points to the center of the local curvature. The local radius of curvature is equal to $1/|\vec{K}|$. It follows from Eq. (30) that $\vec{K} = \partial\vec{T}/\partial\Lambda = \partial(A_i\cos\Lambda - B_i\sin\Lambda)/\partial\Lambda = -\vec{Y}$. It means that $|\vec{K}| = |\vec{Y}| = 1$ and that the trajectory is a great circle [2] on S_5. It follows from $|\vec{T}| = 1$ that the angular distance between points on this great circle is equal to the difference of Λ values of the two tensors that correspond to the points. The endpoints of $\vec{h}$ and $\vec{p}$ can exist at the points with intervals of 60° along the great circle (Fig 7b).

5.2. Infinitesimal rotation

A rotation of stress axes or a fault-slip datum is denoted by the rotation of X. Any 3D rotation can be achieved by the suc-

cessive rotations about the axes of Cartesian coordinates (Fig. 7a). In this case, the principal orientations of X has the expression,

$$Q = \begin{pmatrix} \cos\phi_3 & -\sin\phi_3 & 0 \\ \sin\phi_3 & \cos\phi_3 & 0 \\ 0 & 0 & 1 \end{pmatrix} \begin{pmatrix} \cos\phi_2 & 0 & \sin\phi_2 \\ 0 & 1 & 0 \\ -\sin\phi_2 & 0 & \cos\phi_2 \end{pmatrix}$$
$$\times \begin{pmatrix} 1 & 0 & 0 \\ 0 & \cos\phi_1 & -\sin\phi_1 \\ 0 & \sin\phi_1 & \cos\phi_1 \end{pmatrix}, \quad (31)$$

where ϕ_i is the angle of rotation about the ith axis. In case of $\phi_1 = \phi_2 = \phi_3 = 0$, we have $Q = I$, and X in Eq. (2) is a diagonal matrix with X_{11}, X_{22} and X_{33} being the maximum, intermediate and minimum eigenvalues, respectively. The corresponding eigenvectors are parallel to the 1-, 2- and 3-coordinate axes.

A small rotation of X is denoted by the small movement of Y on S_5, which is denoted further by the tangent vectors, $\partial\vec{Y}/\partial\phi_1$, $\partial\vec{Y}/\partial\phi_2$ and $\partial\vec{Y}/\partial\phi_3$. These three tangent vectors and $\vec{T}$ in Eq. (30) are perpendicular from each other (Supplement). However, there are exceptional cases. When X has axial symmetry ($\Phi = 0$ or 1) and when the rotation axis in the physical space is parallel to the symmetry axis, the tangent vector that corresponds to the rotation vanishes. However, such a rotation is meaningless because the ellipsoid representing X is not affected by the rotation. The points where datum vectors, $\vec{h}$ and $\vec{p}$, can exist are arranged discretely along the $\vec{\Lambda}$ direction on S_5 (Fig. 7b), but the rotation of a datum in the physical space leads to the continuous movement of a Fry arc across this direction (Fig. 7c).

5.3. Finite rotation

Now, we look at the global pattern of the trajectory on S_5 as a function of Q with a fixed Λ value. It is shown in this subsection that the trajectory corresponding to a rotation of X about an arbitrary chosen axis in the physical space is a Lissajous-like curve on S_5. Eq. (31) indicates the rotation by the angle of ϕ_3 about an arbitrarily chosen axis with respect to the principal orientations of X. The direction of this axis is denoted by ϕ_1 and ϕ_2. Therefore, the trajectory corresponding to such a rotation is described by the function, $\vec{Y}(\phi_3)$, with Λ, ϕ_1 and ϕ_2 kept constant.

$\vec{Y}(\phi_3)$ is a complicated function of ϕ_3 (Supplement), but, in short, can be written as

$$\begin{pmatrix} Y_1 \\ Y_2 \\ Y_3 \\ Y_4 \\ Y_5 \end{pmatrix} = \begin{pmatrix} C_1 & D_1 & 0 & 0 & G_1 \\ C_2 & D_2 & 0 & 0 & G_2 \\ 0 & 0 & E_3 & F_3 & 0 \\ 0 & 0 & E_4 & F_4 & 0 \\ C_5 & D_5 & 0 & 0 & G_5 \end{pmatrix} \begin{pmatrix} \cos 2\phi_3 \\ \sin 2\phi_3 \\ \cos\phi_3 \\ \sin\phi_3 \\ 1 \end{pmatrix}, \quad (32)$$

where the components of this square matrix are the functions of Λ, ϕ_1 and ϕ_2. Eq. (32) indicates the periodic change of the components of $\vec{Y}$. Y_3 and Y_4 has the same periodicity, and cycles just with ϕ_3. In contrast, the periodicity of Y_1, Y_2 and Y_5 is two times larger than that of ϕ_3, because the three components include $\cos 2\phi_3$ and $\sin 2\phi_3$. Therefore, the trajectory of $\vec{Y}$ is a spherical Lissajous—a Lissajous curve lying on S_5 (Fig. 8).
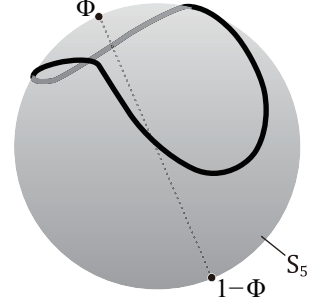

Figure 8: Schematic illustration of a spherical Lissajous (thick line) on S_5. Solid circles depict the antipodal pair of points representing opposite stresses with the shape ratios of Φ and $1 - \Phi$.

The trajectory corresponding to a rotation about an axis in the physical space is a great circle arc [2] upon S_5 only if $\Phi = 1/2$, because antipodal points on S_5 represent the tensors with Φ and $1 - \Phi$ (§4.6). Thus, antipodal points have the same shape ratio only if $\Phi = 1/2$ (Fig. 8). It means that if the tensor to be rotated has an other ratio, the trajectory cannot be a great circle arc [2]. Accordingly, the spherical linear interpolation, $\vec{s}$, in Eq. (28) does not always represent a stress with the same Φ value with the stress(es) corresponding to one or both ends of the interpolated interval.

The same is true for strain tensors. Points along the trajectory on S_5 due to a rotation of ϵ or ϵ' about an axis in the physical space do not have the same shape ratio unless the shape ratio of the strain tensor is 1/2. Consequently, the point obtained as the linear interpolation of two h-vectors, or the 6D ϵ-vectors in Eq. (24), represent a strain whose shape ratio is not always 1/2. Points standing for tensors without the shape ratio at 1/2 do not represent plane strains. That is, the point does not represent a fault-slip datum as long as the vectors do not represent the strain tensors with the eigenvectors in common, The fault-slip data whose n-, v- and b-vectors are permuted have common eigenvectors. The impossibility for the linear interpolation of h-vectors to be a fault-slip datum is contrary to the statement of Shan et al. (2019) who attempted to use the imaginary e-twin datum obtained through the linear interpolation.

6. Dissimilarity classes of reduced stress tensors

Dissimilarity between reduced stress tensors has practical importance (Michael, 1987; Orife and Lisle, 2003). That is, it can be used to judge whether the inversion results from different rock bodies have a significant difference. If it is not, we can argue that the bodies were subjected to more or less the same stress condition.

6.1. Dissimilarity measures

In the formulation of stress inversion using the deviatoric stress-strain space, it is natural to use the angular distance, Θ, on S_5 between the points, $\vec{s}^{(1)}$ and $\vec{s}^{(2)}$ as the dissimilarity of the stresses that are represented by the points (Fig. 10). Yamaji and Sato (2006) called Θ angular stress distance. Since
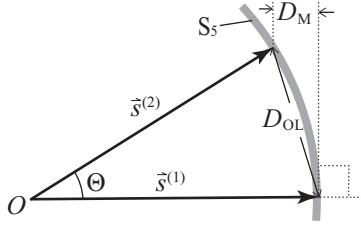
Figure 9: The geometrical interpretations of the dissimilarity measures, D_M, D_{OL} and Θ, of reduced stress tensors. Reduced stress tensors are represented by the endpoints of $\vec{s}^{(1)}$ and $\vec{s}^{(2)}$ on S$_5$, which has the center, O.

Figure 10:

the s-vectors have unit lengths, we have $\Theta = \cos^{-1}\left[\vec{s}^{(1)} \cdot \vec{s}^{(2)}\right]$ (Yamaji and Sato, 2006). Stresses with $\Theta = 0°$ are equivalent with each other; and those with $\Theta = 180°$ are opposite stresses. If a reduced stress tensor changes its principal axes, the distance between the initial and 'roaming' tensor is related to the rotation of the axes. However, it is not easy to evaluate the dissimilarity only from the visual inspection of stress axes in a stereonet, because the dissimilarity depends not only on the angle of rotation but also on stress ratio. The same amount of rotations about different rotation axes can lead to different dissimilarities. For example, a rotation does not change an axially symmetric stress condition ($\Phi = 0$ or 1) if the axis of rotation is parallel to the symmetry axis. The rotation of the stress tensor about its σ_2-axis by the angle, ϕ, leads to $\Theta = \cos^{-1}[3(\cos 2\phi - 1)/6\lambda^2 + 1]$ (Figs. 11a and b). If stress orientations are unchanged, a change only in Φ leads to a different tensor (Fig. 11c).

The dissimilarity measures between reduced stress tensors, D_M and D_{OL}, were proposed by Michael (1987) and Orife and Lisle (2003). We call them Michael and Orife-Lisle distances. Both the distances range from 0 to 2. They are related to each other through the equations (Yamaji and Sato, 2006),

$$D_{OL} = \left|\vec{s}^{(1)} - \vec{s}^{(2)}\right| = 2\sin(\Theta/2) \tag{33}$$

$$D_M = 1 - \vec{s}^{(1)} \cdot \vec{s}^{(2)} = 1 - \cos\Theta = D_{OL}^2/2. \tag{34}$$

The distances, Θ, D_{OL} and D_M, are invariants under coordinate rotations in the physical space.

Θ has an important property. Let Θ be the angular stress distance of a trial stress tensor from the correct solution of stress inversion. Then, the mean misfit angle of the trial tensor for randomly oriented fault planes is approximately equal to Θ (Yamaji and Sato, 2006). That is, we have

$$\left\langle \cos^{-1}(s^{(1)} \cdot s^{(2)}) \right\rangle \approx \Theta,$$

where $s^{(i)}$ is the unit vector indicating the theoretical slip direction of the fault with the unit normal, n, under the i stress; and the mean, $\langle \cdots \rangle$, is taken over all the possible directions of n. Accordingly, we can tell the representative difference in the slip directions under two stresses using Θ.

D_{OL}^2 is proportional to the mean difference of shear stresses on randomly oriented fault planes as follows. The shear stress
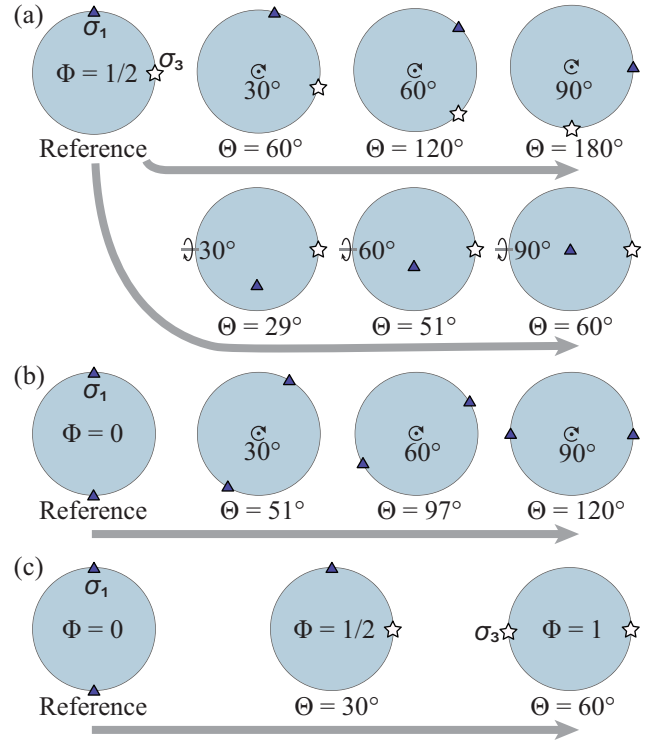

Figure 11: Stereoplots showing the variation of Θ corresponding to the rotation of stress axes from the reference tensors. The variation associated with the progressive rotations of triaxial (a) and axial (b) stress tensors. (c) The variation associated with the change in Φ with fixed principal orientations. Changes of stress conditions in (c) and those in (a, b) correspond to the movement of a point along the Λ-direction the remaining directions, respectively, on S$_5$ (Fig. 7b).

9

on the fault with the unit normal, n, can be expressed as the vector quantity, τ, whose length equals the shear stress magnitude on the reduced stress tensor, ς. The sense of shear is denoted by the direction of τ. Since this vector is the orthogonal projection of traction, ςn, we have $\tau = [\text{diag}\,(1, 1, 1) - nn^\top]\varsigma n$, where the contents of the square brackets represents the projection (e.g., Meyer, 2000, Eq. 5.6.2). Sato (2012b) derived the equation,

$$\left\langle \tau^{(1)} - \tau^{(2)} \right\rangle = \frac{2}{5} D_{\mathrm{OL}}^2,$$

where $\tau^{(i)}$ is the vectorial shear stress on the fault with the unit normal, n, under the ith reduced stress tensor. Combining this and Eq. (34), we obtain $\langle \tau^{(1)} - \tau^{(2)} \rangle = 4D_{\mathrm{M}}/5$.

6.2. Dissimilarity classes

Orife and Lisle (2003) proposed a classification scheme for the dissimilarities. As a result, they defined 'very similar,' 'similar,' 'different' and 'very different' classes as the intervals, $D_{\mathrm{OL}} = 0.00$–0.66, 0.68–1.01, 1.01–1.71 and 1.71–2.00, respectively. The classification scheme was based on $P_{\mathrm{OL}}(D_{\mathrm{OL}})$, the probability density function of D_{OL} for tensor pairs randomly chosen from the uniform distribution of reduced stress tensors. Unfortunately, their reasoning to settle the intervals of the classes was groundless. Here, we give new meaning to the classes and adjust the boundary values.

The uniform distribution of reduced stress tensors is represented by a uniform distribution of points on S_5. This geometrical interpretation yields the analytical expression (Yamaji and Sato, 2006) (Fig. 12a),

$$P_{\mathrm{OL}}(D_{\mathrm{OL}}) = \frac{3}{16} D_{\mathrm{OL}}^3 (4 - D_{\mathrm{OL}}^2).$$

Orife and Lisle (2003) obtained a good approximation of this equation using a Monte Carlo technique. This distribution has the mean and standard deviation, $m = \int_0^2 D_{\mathrm{OL}} P_{\mathrm{OL}}(D_{\mathrm{OL}})\, dD_{\mathrm{OL}} = 48/35 \approx 1.37$ and $sd = \left[\int_0^2 (m - D_{\mathrm{OL}})^2 P_{\mathrm{OL}}(D_{\mathrm{OL}})\, dD_{\mathrm{OL}} \right]^{1/2} = (146/1225)^{1/2} \approx 0.35$. Orife and Lisle (2003) determined the class boundaries at $D_{\mathrm{OL}} = m - 2sd$, $m - sd$ and $m + sd$ (Fig. 12a).

However, the choice of a dissimilarity measure is arbitrary. The probability density function of D_{M} for the uniform distribution is $P_{\mathrm{M}}(D_{\mathrm{M}}) = \frac{3}{4} D_{\mathrm{M}}(2 - D_{\mathrm{M}})$ with the mean and standard deviation, 1 and ~0.45, which corresponds to $D_{\mathrm{OL}} \approx 1.41$ and 0.95, respectively. That of Θ is

$$P_\Theta(\Theta) = \frac{3}{4} \sin^3 \Theta \qquad (35)$$

with the mean and standard deviation, $90°$ and ~$28°$, corresponding to $D_{\mathrm{OL}} \approx 1.41$ and 0.48, respectively (Fig. 12b) (Yamaji and Sato, 2006). Therefore, their reasoning to determine the class boundaries depends on the choice of a dissimilarity measure. The mean and standard deviation of $P_{\mathrm{OL}}(D_{\mathrm{OL}})$ are not suitable to reason out the classification scheme.

Here, we present a new way of reasoning and redefine the class boundaries. That is, the class boundaries are defined with
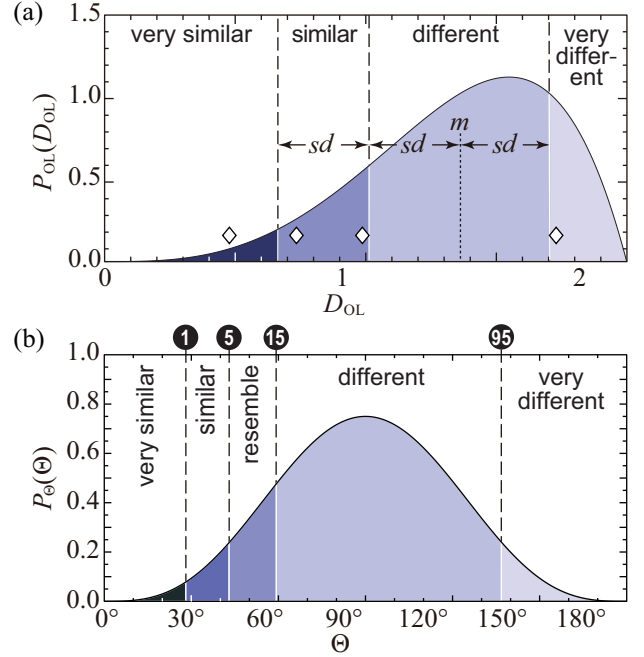

Figure 12: The probability density functions of D_{OL} (a) and Θ (b) for randomly chosen tensors. Boldface letters indicate the dissimilarity classes of reduced stress tensors of (Orife and Lisle, 2003) (a) and this study (b). The mean and standard deviation of $P_{\mathrm{OL}}(D_{\mathrm{OL}})$ are denoted by m and sd in (a). Diamonds indicate the D_{OL} values corresponding to the class boundaries in (b), where the dissimilarity classes with the boundaries at the 1, 5, 15 and 95 percentile points.

the 1, 5, 15 and 95 percentiles of the probability density function of the dissimilarity. Eq. (35) gives the cumulative distribution function,

$$F(\Theta) \equiv \int_0^\Theta P_\Theta(t)\, dt = \frac{1}{4} \left(\cos^3 \Theta - 3 \cos \Theta + 2 \right),$$

with which we defines the class boundaries. That is, solving te equations, $F(\Theta) = 0.01, 0.05, 0.15$ and 0.95, we have the boundary values, $\Theta \approx 28.09°, 43.17°, 59.26°$ and $136.83°$, respectively (Fig. 12, Table 9). The definitions of the class boundaries in terms of percentile points are independent from the choice of a dissimilarity measure. That is, Eqs. (33) and (34) transform those class boundaries to the same percentile points of $P_{\mathrm{OL}}(D_{\mathrm{OL}})$ and $P_{\mathrm{M}}(D_{\mathrm{M}})$.

When the classes are defined in terms of percentiles, they are practically convenient. If 'very similar' stresses are obtained by the stress inversion of data sets from two rock masses, it is highly probable that the masses experienced the same stress condition, because the probability for two stresses in the 'very similar' class by chance is only 1%. The probability for the stress tensors in the 'similar' class to have $\Theta < 43.17°$ by chance is smaller than 5%. So, if stresses detected from two rock masses are 'similar' to each other, the masses experienced probably the same or at least similar stress conditions. The 'resemble' class is defined, here, because such a 5% confidence limit is sometimes too strict for practical tectonic studies.

10

7. Stress inversion of faults

The majority of the current inversion schemes of fault data are based on the Wallace-Bott hypothesis, allowing us to use Fry arcs or the paired equation and inequality in (27). Gushchenko (1973) and Carey and Brunier (1974) pioneered the paleostress analysis based on the hypothesis. Several researchers challenged the hypothesis (Pollard et al., 1993; Nieto-Samaniego and Alaniz-Alvarez, 1997; Pascal, 2002; Lisle, 2013; Lejri et al., 2015, 2017). Those studies showed the situations where the hypothesis has discrepancies typically as large as a few degrees between the direction of maximum resolved shear stress and the slip direction. The inversion scheme that is not based on the hypothesis but on the slip tendency (Morris et al., 1996) were proposed recently (McFarland et al., 2012; Tranos, 2015), which is discussed in §7.3.

7.1. The linear programming problem corresponding to the inversion

The idea of the inversion by Fry (1999) can be formulated as a linear programming problem. That is, the s-vector representing the optimal stress is the solution of the linear system,

$$\vec{h}^{(1)} \cdot \vec{s} > 0, \dots, \vec{h}^{(N)} \cdot \vec{s} > 0, \tag{36}$$

$$\vec{p}^{(1)} \cdot \vec{s} = 0, \dots, \vec{p}^{(N)} \cdot \vec{s} = 0 \tag{37}$$

where N is the number of data, $\vec{h}^{(i)}$ and $\vec{p}^{(i)}$ are the h- and p-vectors of the ith datum (Eq. 27). The s-vector that minimizes $\sum_{i=1}^{N}[\vec{p}^{(i)} \cdot \vec{s}]^2$ with the constraints in (36) represents the optimal stress in a least square sense. Given a homogeneous data set, the optimal s-vector is determined through the method of Languages multiplier. That is, the orientation-distribution matrix,

$$\sum_{i=1}^{N} \vec{p}^{(i)} [\vec{p}^{(i)}]^\top, \tag{38}$$

characterizes the distribution of the p-vectors (Borradaile, 2003, Eq. 10.11). And, the eigenvector corresponding to the minimum eigenvalue is the optimal s-vector.

It follows from the inequalities in (36) that $\vec{s}$ makes acute angles with all the h-vectors; and define the feasible region for $\vec{s}$. Linearly independent h-vectors are always in a hemisphere if $N \leq 5$ because the deviatoric stress-strain space has five dimensions. In this case, the feasible region does exist whether or not the conditions in Eq. (37) are fulfilled by $\vec{s}$ in the feasible region. The sixth h-vector in the other hemisphere violates the condition for the feasible region to exist. That is, the condition in (36) is always fulfilled by five data, but can be violated by six data.

On the other hand, it follows from the simultaneous equations (Eq. 37) that $\vec{s}$ is perpendicular to the p-vectors (Fig. 14a). In other words, $\vec{s}$ is the intersection of the hyperplanes [4] perpendicular to the p-vectors. Since the deviatoric stress-strain space is five-dimensional, linearity independent four p-vectors can be perpendicular to a s-vector: the four p-vectors and s-vector make up the base vectors of the space. In this case, the
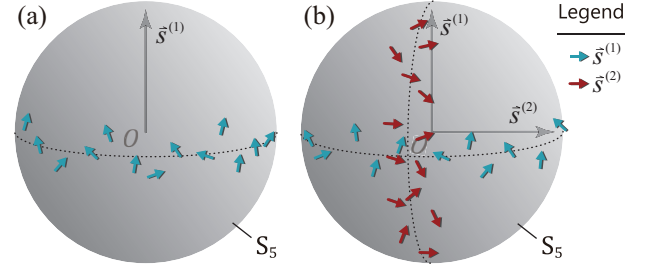

Figure 13: Schematic illustrations of datum vectors on S_4 corresponding to homogeneous (a) and heterogeneous (b) fault-slip data. The stresses responsible for the faulting are indicated by long arrows. The positions of short black arrows on the spheres indicate the endpoints of p-vectors which are scattered along great circles [4] with the poles indicated by the arrows. The points are aligned along the great circle if the data are free from perturbations. The directions of the short arrows indicate the h-vectors, and show the distinction whether the data came from the stresses represented by $\vec{s}^{(1)}$ and $\vec{s}^{(2)}$. Short arrows in the group of $\vec{s}^{(i)}$ make acute angles with $\vec{s}^{(i)}$ ($i = 1$ or 2).

Figure 14:

s-vector is readily obtained using the equation,

$$\vec{s} = \frac{1}{A} \det \begin{pmatrix} p_1^{(1)} & \cdots & p_1^{(4)} & \vec{e}^{(1)} \\ \vdots & & \vdots & \vdots \\ p_5^{(1)} & \cdots & p_5^{(4)} & \vec{e}^{(5)} \end{pmatrix}, \tag{39}$$

where $p_j^{(i)}$ is the jth component of the ith p-vector, $\vec{e}^{(1)}$ through $\vec{e}^{(5)}$ in the rightmost column are the orthonormal bases of the five-dimensional deviatoric stress-strain space, and A is the normalizing factor making the right-hand side of this equation into a unit vector (Shurman, 2016, p. 421). However, this equation leaves the direction of $\vec{s}$ uncertain, because both $+\vec{s}$ or $-\vec{s}$ satisfy Eq. (37). Instead, the sign is determined by the inequalities (36). At least four p-vectors are required to determine the optimal $\vec{s}$. In case of $N < 4$, Eq. (37) is an under-determined system, meaning that the s-vector cannot be uniquely determined. In case of $N > 4$, it is an over-determined one. That is, the hyperplanes perpendicular to the p-vectors can intersect various points on S_5. Even in this case, we can get the optimal solution that satisfies the equations (37) in a least-square sense.

Several researchers adopted the aforementioned approach (Fry, 1999, 2001; Shan et al., 2003, 2004b). They determined, first, the optimal s-vector(s) from Eq. (37) in a least square sense, first; and, second, the directions of the vector(s). Given a heterogeneous data set, the points on S_5 indicated by p-vectors are scattered along two or more great circles [4] (Fig. 14b). Shan and his coworkers employed fuzzy clustering to separate stresses from such a set (Shan et al., 2004b). That is, they fitted one or more great circles [4] to the points on S_5 indicated by the p-vectors.

The approach is successful for homogeneous data. However, given heterogeneous ones, it is theoretically inferior to those using Fry arcs (§7.2) with respect to the accuracy and resolution of the stress inversion. However, the opposite may be true depending on the computational grid, numerical optimization schemes and others of computer programs. The shortcoming of

11

the approach comes from the fact that it does not treat the equality and inequality constraints (Eqs. 36 and 37) equally. The latter is used only to choose the sign(s) of the optimal solution(s) that have been determined from the former. Stress tensors are determined primarily only from p-vectors, where the information of h-vectors are not used. Note that p-vectors along different great circles [4] are intermingled around the intersections of the circles (Fig. 14), but the their h-vectors are the indicators of their great circles. Since the approach does not utilize the indicators when great circles are fitted, the resolution and accuracy of the approach are spoiled by the intermingled data points more than the inversion schemes that use both p- and h-vectors equally.

7.2. Inversion schemes using Fry arcs

Given N data, the same number of Fry arcs are determined using Eq. (27). That is, we have the N constraints,

$$\begin{cases} \vec{h}^{(1)} \cdot \vec{s} > 0 \\ \vec{p}^{(1)} \cdot \vec{s} = 0 \end{cases} \cdots, \begin{cases} \vec{h}^{(N)} \cdot \vec{s} > 0 \\ \vec{p}^{(N)} \cdot \vec{s} = 0 \end{cases},$$

for the stress inversion, where each pair defines a Fry arc. The inversion scheme using Fry arcs treat the equality and inequality constraints equally.

If an exactly single stress tensor results in faulting, the Fry arcs from the faults meet at the point on S_5 that represents the stress (Fig. 15a). However, natural data are subjected to perturbations to some extent. Measurement errors shifts Fry arcs on S_5 even if the data are homogeneous. The arcs do not meet at a single point, but make intersections. The center of the cluster made by the intersections represents the optimal stress (Fig. 15b). Given a heterogeneous data set, the intersections make two or more dense clusters (Fig. 15c), and the cluster centers indicate the optimal stresses.

Several inversion schemes employ the idea analogous to the generalized Hough transform (Ballard, 1981), a technique of image processing to recognize plural objects in an image, to cope with heterogeneous data. That is, the dihedra (Angelier and Mechler, 1977), y-R diagram (Gómez, 1986), trihedra (Lisle, 1987), multiple inverse (Yamaji, 2000), Ginko (Yamaji, 2003), Hough transform (Yamaji et al., 2006) and Gauss (Žalohar and Vrabec, 2007) methods superpose Fry arcs to search for their intersections. Among them the right-dihedra method is the most accessible because it requires only a stereonet. It have been applied to natural data from various areas, and have been employed for the visualization of the results of newly developed schemes (e.g., Nemcok et al., 1999; Lisle et al., 2001; Shan et al., 2019). The method superposes "beachball patterns" on a stereonet. The patterns are the shadows of Fry arcs projected onto a 2D plane. The limitation of the method, including the incapability of determining stress ratio, comes from this projection. Suppose a few clumpy clouds casting their shadows onto the ground. Even if the shadows overlap each other on the ground, it is not difficult to recognize each lamps from an airplane. Generally, it is difficult to separate objects that exist in a high dimensional space from their projections in a lower dimensional space. The objects should be
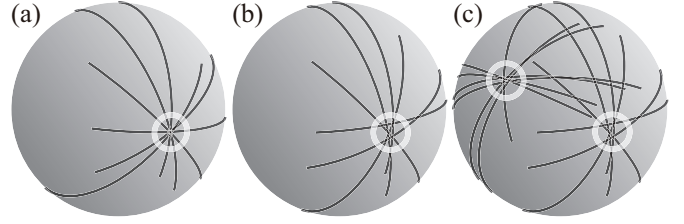

Figure 15: Schematic illustrations of Fry arcs (thick lines) on S_5. (a) Fry arcs corresponding to homogeneous data without perturbations. (b) Those of homogeneous one with perturbations. (c) Heterogeneous data resulting from two stresses. White circles indicate the clusters made by the intersections of Fry arcs.

recognized in the high dimensional one. The multiple inverse and Hough transform methods were devised not to spoil the separation of Fry arcs when they are projected onto a 2D plane for the visualization of inversion results.

The Fry arcs of heterogeneous data have a great number of intersections, which act as noise to hinder the stress inversion (Fig. 15c). The multiple inverse method (Yamaji, 2000; Otsubo and Yamaji, 2006; Otsubo et al., 2008) reduces the noises and enhances significant solutions by ignoring the areas on S_5 where only a few Fry arc pass. The method is used to invert not only geological fault–slip data but seismological focal mechanism data (e.g., Kassaras and Kapentanidis, 2018). Sato (2012c) attempted to reduce the computation time of the method using Eq. (39). The capability of the multiple inverse and Hough transform methods to deal with heterogeneous data enables the bedding tilt test of paleomagnetism combined with the methods to determine the timing of stress(es) relative to folding from fault-slip data collected in folded strata (Yamaji et al., 2005; Tonai et al., 2011).

7.3. Unfavorably oriented faults

Faults nearly parallel to a stress axis are said to be unfavorably oriented, because shear stresses acting on the faults are small even if $\Delta\sigma$ is not small. The faults can still be activated by the lubrication of the fault surfaces by high pressure fluids or weak gouge. Data from the faults make the stress inversion result unstable if data from such faults are dominant. The instability arises from the fact that nearly opposite stresses can result in fault-slip data with similar directions (Fig. 17a). Furthermore, small perturbations affecting fault-slip data can lead to an abrupt jump of an inversion result between the opposite stresses, if data from unfavorably oriented faults are dominant.

The origin of the instability has a geometrical interpretation in the deviatoric stress-strain space. It comes from the fact that the ends of a Fry arc have singularity for the misfit angle on the fault corresponding to the arc as follows. Firstly, shear stress on an unfavorably oriented fault is small. It follows from Eq. (29) that $\vec{s} \cdot \vec{h} \approx 0$, meaning that $\vec{s}$ and $\vec{h}$ make an angle of $\sim 90°$. Therefore, the point exists near an end of the Fry arc, because a Fry arc has a length of $180°$, and is centered by $\vec{h}$. Secondly, due to the geometrical relation in Fig. 5 about a misfit angle and the Fry arc, misfit contours meet at the ends of the
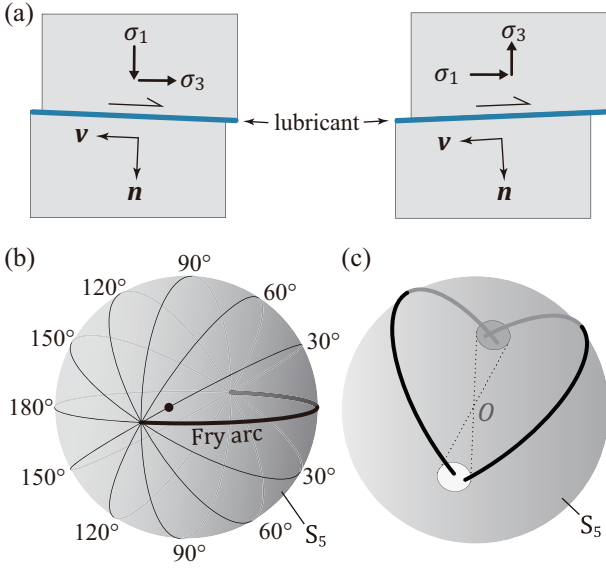
Figure 16: (a) Unfavorably oriented normal and thrust faults with similar attitudes and slip directions under normal and reverse faulting stress regimes. (b) Schematic illustration of the contours of misfit angles (thin lines) on S_5 (Fig. 5). For example, if the point denoted by the solid circle represents the stress that activated a fault, the misfit angle on the fault represented by the Fry arc (thick line) is 30°. (c) Schematic illustrations of the Fry arcs of unfavorably oriented faults. The arcs approach or intersect with each other around antipodal points on S_5. Their intersection jumps between the points by a small perturbation.
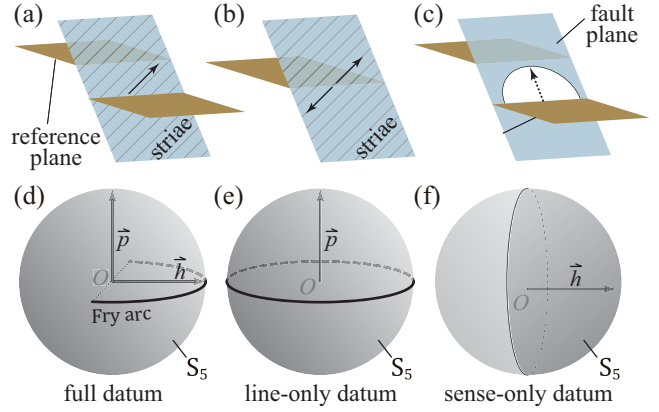
Figure 17:

Figure 18: Schematic illustrations of faults providing full datum and two types of incomplete fault-slip data (a–c) and corresponding solid figures lying on S_5 (d–f). Arrow in (a) indicates the slip direction, v, of the footwall. Arrows in (b) indicate the possible ones. White fan in (c) indicates the range of possible v directions, and the dotted arrow points the center of the range. A key bed, dike, etc., can be the reference plane for us to judge the sense of faulting (a) or to recognize this central direction (c).

arc (Fig. 17b). Fry arcs are slightly shifted by small measurement errors in fault attitudes and slip directions; and the point, $\vec{s}$, moves slightly on S_5 by a small perturbation in the state of stress. Both of these small effects result in rapid changes of the misfit angle of an unfavorably oriented fault, resulting in the instability. In addition, the lengths of the arcs (180°) are enough for their intersections to jump between antipodal points by the perturbations (Fig. 17c).

Gephart and Forsyth (1984) addressed this problem. They considered that the problem arises by using the misfit angles as the residuals of the inversion. And, they replaced the misfit angles with the minimum angles of fault-slip data to eliminate the misfit angles under a trial stress tensor. However, this redefinition of the residuals does not solve the problem: The instability arises by the nature of the stress inversion (Figs. 17b, c). The rotation of a fault-slip datum proposed by Gephart and Forsyth (1984) shifts a Fry arc to make it pass through the point on S_5 corresponding to a trial stress. That is, the Fry arc in Fig. 17b is moved to the point indicated by the solid circle in the figure. However, both the antipodal points on S_5 represented by the centers of the dark and white areas in Fig. 17c are in the vicinity of Fry arcs. This example demonstrates that the redefinition does not remove the instability from the inversion.

The stress inversion based on slip tendency (Morris et al., 1996) is not either, because the slip tendency neglects the lubrication effect (Sato, 2016). The tendency is not proportional to, but has a positive correlation with τ (Eq. 29). So, the inversion

based on slip tendency (McFarland et al., 2012; Tranos, 2015) makes little of such stresses that have corresponding s-vectors near the ends of Fry arcs. As a result, the lubrication effect that can lead to the instability is virtually ignored, and the terminal parts are cut off from the arcs. The proposal to use shear stress magnitudes for the residuals by Angelier (1990) also takes little account of the effect.

7.4. Incomplete fault-slip datum

An ordinary fault-slip datum consists of the information of the attitude of a fault plane, the orientation of striae and sense of faulting to uniquely determine n and v of the fault. If all the information is obtained from a fault, the fault data is called a full datum (Fig. 18a). Without offset markers such as displaced strata, the sense of faulting can be judged from asymmetric slickenside striations (e.g., Petit, 1987). Such a fault provides a complete datum as well. Data with insufficient information are said to be incomplete. Sato (2006) called the data without the information of fault sense line-only data (Fig. 18b). And, he called those with unknown fault senses line-only data (Fig. 18c). Incomplete data are collected more often than complete data in practice. Active fault studies are popular in Japan, but they have not routinely described the slip directions of faults. Consequently, they have produced sense-only data, clues to Holocene and late Pleistocene stress field (Tsutsumi et al., 2012). Therefore, it is important to develop an inversion scheme to deal with incomplete data.

Lisle et al. (2001) pioneered the stress inversion of sense-only data. They noticed the vertical components of the displacements of (oblique) normal and reverse faults. The sign of the components indicate their up- and downward displacements of the footwalls (Fig. 18c). The signs should be concordant with the resolved shear stresses along their dip directions, which depend on a trial stress tensor. Thus, sense-only data can

13

be inverted to determine the optimal stress. That is, those constraints can be expressed by the inequalities (36) provided that the h-vectors are computed from the unit vector indicated by the dotted arrow in Fig. 18c, though they did not employed the geometrical interpretations of the inequalities.

Shan et al. (2004a) adopted the "slack variables" of linear programming (e.g., Boyd and Vandenberghe, 2009) to transform an inequality constraint from a sense-only datum to an equality constraint, thereby they devised an inversion scheme. Every such datum has a slack variable, which is an unknown to be determined by the inversion along with the optimal stress. So, the number of unknown quantities increases unfortunately with the number of data, making the inversion difficult.

The methods of Lisle et al. (2001) and Shan et al. (2004a) have a limitation that all faults must have reference planes with the same attitudes to judge whether they have normal or reverse senses. For example, if marker beds are the references, all of them should be horizontal. However, the marker beds generally have various attitudes. In addition, sense-only data are as common as line-only data, which the methods cannot deal with. Sato (2006) solved these problems by adapting the Hough transform method of Yamaji et al. (2006), and succeeded in dealing with complete data and two types of incomplete data.

Sato (2006) found the solid figures lying on S_5 corresponding to the incomplete fault-slip data types. That is, the great circle [4] perpendicular to $\vec{p}$ represents a line-only datum (Fig. 18d), where the circle is composed of the two Fry arcs that are computed from the fault attitude, $\boldsymbol{n}$, and the possible slip directions, $\pm\boldsymbol{v}$. And, the hemisphere centered by $\vec{h}$ represents a sense-only datum (Fig. 18e), where $\vec{h}$ is computed from the center of the possible slip directions (Fig. 18c). Full data are represented by Fry arcs. So, the optimal stress(es) can be determined by superimposing those figures upon S_5: The clustered intersections of the figures indicate the optimal stress(es). In addition, the method of Sato (2006) is capable of dealing with the various attitudes of reference planes, making a fold test possible (Tonai et al., 2011).

8. The side effects of lacking the coordinate invariance

Fry (1999, 2001) pioneered the geometrical interpretation of the stress inversion by means of high dimensional parameter space, but his formulation is unfortunately affected by the choice of a coordinate system due to the lack of the factors, $1/\sqrt{2}$ and $\sqrt{2}$, in Eq. (24). This gives rise to the variable lengths and angles of the 5D and 6D vectors depending on the choice of a coordinate system in the physical space (Fig. 19). The 5D datum vector of Shan et al. (2003), which corresponds to our $\vec{p}$ but lacks the factors, has a variation in length from ∼0.7 to 1.2, which spoils the accuracy and resolution of the inversion (Sato and Yamaji, 2006b). The factors cancel out the variations of the length and angles, and make our formulation agree with the principle of coordinate invariance.

8.1. Inaccuracy

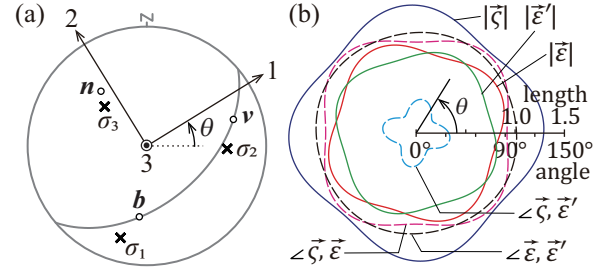Shan et al. (2003) developed an inverse method based on the

Figure 19: (a) Lower-hemisphere stereoplot showing a stress condition ($\Phi = 1/2$) and a fault-slip datum denoted by $\boldsymbol{n}$, $\boldsymbol{v}$ and $\boldsymbol{b}$. The stress axes are indicated by crosses. The first and second coordinates lie on the horizontal plane, and the direction of the former is denoted by θ. (b) Polar plot showing the variation of the lengths and angles of $\vec{\varsigma}$, $\vec{\epsilon}$ and $\vec{\epsilon}'$ that are evaluated without the factors, $1/\sqrt{2}$ and $\sqrt{2}$, in Eq. (24) for the case of the stress condition and fault-slip datum in (a).

formulation of Fry (1999). They used the 5D datum vector,

$$\vec{q} = (n_1b_1 - n_3b_3, n_2b_2 - n_3b_3,$$
$$n_2b_1 + n_1b_2, n_3b_1 + n_1b_3, n_3b_2 + n_2b_3)^{\mathrm{T}} \quad (40)$$

to invert fault-slip data. A numerical experiment using a million orthonormal pairs of $\boldsymbol{n}$ and $\boldsymbol{b}$ with random orientations showed that $|\vec{q}|$ had the mean and standard deviation at 1.0046 and 0.0835. The origin of this variation is explained as follows. The vector in Eq. (40) corresponds to our $\vec{p}$ in Eq. (25) through the equation,

$$\vec{q} = \begin{pmatrix} 0 & -1 & 0 & 0 & 0 \\ \sqrt{3}/2 & -1/2 & 0 & 0 & 0 \\ 0 & 0 & 0 & 0 & 1 \\ 0 & 0 & 0 & 1 & 0 \\ 0 & 0 & 1 & 0 & 0 \end{pmatrix} \vec{p}. \quad (41)$$

Given the unit vectors, $\boldsymbol{n}$ and $\boldsymbol{b}$, $\vec{p}$ indicates a point on S_5 (Eq. 26). Thus, Eq. (41) says that $\vec{q}$ indicates a point on a hyperellipsoid. These solid figures are analogous to a unit sphere and strain ellipsoid. That is, the square matrix in Eq. (41) represents a deformation, and we refer the deformation gradient tensor, $\boldsymbol{F}$, to this matrix. Then, the right Cauchy-Green tensor, $\boldsymbol{B} = \boldsymbol{F}\boldsymbol{F}^{\mathrm{T}}$, represents the quadratic strain: The principal strains and strain axes are the square-roots of the eigenvalues and the eigenvectors of $\boldsymbol{B}$ (Malvern, 1969). That is, we have the principal strains, $\sqrt{6}/2, 1, 1, 1$ and $\sqrt{2}/2$, indicating an anisotropic deformation. Lengths and angles are generally changed by such a deformation. The choice of coordinate directions in the physical space affects the components of $\boldsymbol{n}$ and $\boldsymbol{b}$, leading to the variable lengths and angles of the q-vectors. If, on the other hand, $\vec{q}$ is a unit vector, the corresponding $\boldsymbol{n}$ and $\boldsymbol{b}$ in the physical space do not make an orthonormal system except for some cases, e.g., $\boldsymbol{n} = (0, 0, 1)^{\top}$ and $\boldsymbol{b} = (1, 0, 0)^{\top}$.

The variable length gives rise to inaccuracy to the inverse method. That is, in this case the matrix corresponding to Eq. (38) has the form, $\boldsymbol{M} = \sum_{i=1}^{N} \vec{q}^{(i)}[\vec{q}^{(i)}]^{\top}$. An orientation-distribution matrix characterizes the orientation distribution of

unit vectors, but M is not an orientation-distribution matrix due to the variable lengths of the q-vectors. Instead, the quantity, $I - M$, is known as a moment of inertia tensor (e.g., Landau and Lifshitz, 1976, p. 99), where I is an identity matrix. The eigenvector corresponding to the minimum eigenvalue of an orientation-distribution matrix was identified with the vector representing the optimal stress in §7.1. However, a moment depends generally on the lengths of moment arms. Consequently, not only the orientation distribution of the q-vectors but also their variable lengths affect the eigenvectors of M, giving rise to the inaccuracy of the inversion. The variation comes from the fact that the formulation using the datum vector in Eq. (40) lacks the coordinate invariance.

8.2. *Anisotropic resolution*

The lack of the coordinate invariance gives rise to the anisotropic resolution of the stress inversion. A numerical experiment was carried out to compare the formulation with and without the factor $1/\sqrt{2}$ in Eq. (6) using a synthetic, heterogeneous fault-slip data set (Fig. 20a). A hundred faults were assumed to be activated by Stress A with σ_1-axis at 090°/00°, σ_3-axis at 000°/90° and $\Phi = 1/2$, and another hundred by Stress B with σ_1-axis at 180°/45°, σ_3-axis at 000°/45° and $\Phi = 1/2$. The stresses had the σ_1 orientations and stress ratios in common and $\Theta = 90°$: They are classified into 'different' stresses (Table 2). We chose those stresses because their corresponding 5D vectors, $\vec{s}_A = (0, -1, 0, 0, 0)^T$ and $\vec{s}_B = (0, 0, 1, 0, 0)^T$, had a sharp difference in the absolute values of the first and second components, which are affected by the factor of $1/\sqrt{2}$. The fault planes were randomly oriented; and the slip directions were calculated according to the Wallace-Bott hypothesis. Gaussian perturbations with the zero mean and the standard deviation of 15° were imposed on the slip directions.

The data set was processed with the fast multiple inverse method (Sato, 2012a), which used a computational grid of reduced stress tensors as the candidates of optimal solutions. To see the effect of the factor of $1/\sqrt{2}$, two types of grids were examined. The first one consisted of 60,000 points uniformly distributed over S_5 using the formulation with the factor (Yamaji and Sato, 2011). The lack of the factor brings about the distortion of this distribution (Sato and Yamaji, 2006b, Fig. 7) analogous to the deformation represented by Eq. (41). Both the grids consisted of the same number of grid points, but the intervals of the points were not uniform in the second one due to the distortion.

As a result, it was found that the factor of $1/\sqrt{2}$ gives rise to the anisotropic detectability of stresses. The result of the inversion with the factor is shown in Fig. 20b, where the stresses are depicted by the clusters of σ_1 orientations. The two clusters had similar densities, indicating the stresses were equally significant, consistent with the fact that the synthetic data were the mixture of the data sets with the same number of data. In contrast, Stress B is indicated by a smaller cluster compared to Stress A in Fig. 20c. It means that Stress A was detected more easily than Stress B using the distorted computational grid. Such inequality spoils the resolution of stress inversion.

9. Summary

A point in the deviatoric stress-strain space has a one-to-one correspondence with a symmetric, deviatoric tensor. In addition, complete and incomplete fault-slip data have corresponding solid figures in the space. The correspondence allows us to interpret the inversion as a geometrical problem in the space.

Since the geometric relations of the solid figures and the points representing stresses are invariant under the coordinate rotations in the physical space, the relations give a clear perspective to develop the inversion techniques to deal with heterogeneous data from the interpretation. In addition, the stress inversion using the space has isotropic resolution thanks to the invariance. In formulation without the coordinate invariance, equations presented in this article must have the correction factors that denote the distortion of the parameter space employed in the formulation.

The dissimilarity classes of reduced stress tensors were redefined in terms of a random distribution of points in the space which represent the random distribution of reduced stress tensors.

Supplementary material

The supplementary material that details the equations of the trajectories on S_5 can be found at https://dx.doi.org/XXXXX

Angelier, J., 1979. Determination of the mean principal directions of stresses for a given fault population. Tectonophysics 5, T17–T26.

Angelier, J., 1984. Tectonic analysis of fault slip data Sets, J. Geophys. Res. 98, 5835–5848,

Angelier, J., 1990. Inversion of field data in fault tectonics to obtain the regional stress—III. A new rapid direct inversion method by analytical means. Geophys. J. Int. 103, 363–376.

Angelier, J., 1994. Fault slip analysis and paleostress reconstruction. In, Hancock, P.L., ed., Continental Deformation, Pergamon Press. Oxford, 53–100.

Angelier, J., Goguel, J., 1979. Sur une méthode simple de d'etermination des axes principaux des contraintes pour une population de failes. C.R. Hebd. Seances Acad. Sci. D288, 307–310.

Angelier, J., Manoussis, S., 1980. Classification automatique et distinction des phases superposées en tectonique de failles. C.R. Acad. Sci. D290, 651–654.

Angelier, J., Mechler, P., 1977. Sur une méthode graphique de recherche des contraintes principales également utilisable en tectonique et en séismologie: la méthode des dièdres droits. Bull. Soc. Geol. Fr. 19, 1309–1318.

Aris, R., 1989. Vectors, Tensors and the Basic Equations of Fluid Mechanics. Dover, New York.

Arthaud, F., 1969. Methode de determination graphique des directions de raccourcissement, d'allongement et intermediaire d'une population de failles. Bull. Soc. Géol. Fr. 7, 729–737.

Arthaud, F., Mattauer, M., 1969. Exemples de stylolites d'origine tectonique dans le Languedoc, leurs relations avec la tectonique cassante. Bull. Soc. Géol. Fr. 7, 738–744.

Axen, G.J., Luther, A., Selverstone, J., 2015. Paleostress directions near two low-angle normal faults: Testing mechanical models of weak faults and off-fault damage. Geophere 11, 1996–2014.
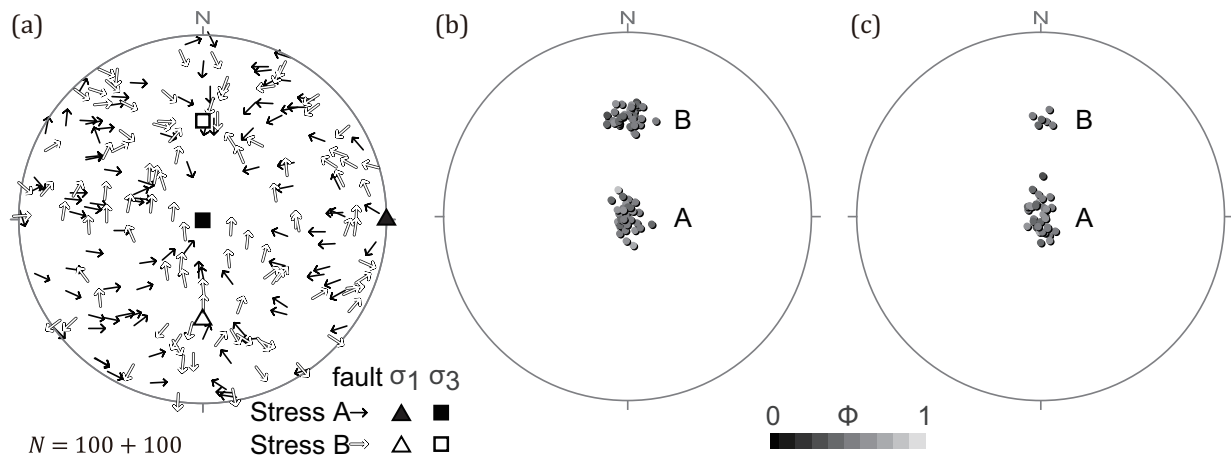
Figure 20: (a) The tangent-lineation diagram showing the artificial fault-slip data composed of 100 faults activated by Stress A and the other 100 by Stress B. (b) The optimal σ_3-axes obtained by using the computational grid on the deviatoric stress-strain space of Sato and Yamaji (2006a). (c) Those obtained by using the Fry's (1999, 2001) formulation. The grayscale indicates the stress ratio. Equal-area and lower-hemisphere projections.

Ballard, D.H., 1981. Generalizing the Hough transform to detect arbitrary shapes. Pattern Recognition 13, 111–122.

Borradaile, G,J., 2003. Statistics of Earth Science Data: Their Distribution in Time, Space and Orientation. Springer, Berlin.

Bott, M.H.P., 1959. The mechanics of oblique slip faulting. Geol. Mag. 96, 109–117.

Boyd, S., Vandenberghe, L., 2009. Convex Optimization. Cambridge Univ. Press, Cambridge.

Carey, E. and Brunier, B., 1974. Analyse théorique et numérique d'un modèle mécanique élémentaire appliqué à l'étude d'une population de failles. C.R. Sci. Acad. Sci. D279, 891–894.

Célérier, B., Etchecopar, A., Bergerat, F., Vergely, P., Arthaud, F., Laurent, P., 2012. Inferring stress from faulting: From early concepts to inverse methods. Tectonophysics 581, 206–219.

Cladouhos T.T. Allmendinger, R.W., 1993. Finite strain and rotation from fault-slip data. J. Struct. Geol. 15, 771–784.

Conel, J.E., 1962. Studies of the development of fabrics in some naturally deformed limestones. PhD thesis, California Institute of Technology.

Etchecopar, A., Vasseur, G., Daignieres, M., 1981. An inverse problem in microtectonics for the determination of stress tensors from fault striation analysis. J. Struct. Geol. 3, 51–65.

Fry, N., 1999. Striated faults: visual appreciation of their constraint on possible paleostress tensors. J. Struct. Geol. 22, 441–452.

Fry, N., 2001. Stress space: striated faults, deformation twins, and their constraints on paleostress. J. Struct. Geol. 23, 1–9.

Gauthier, B., Angelier, J., 1985. Fault tectonics and deformation: a method of quantification using field data. Earth Planet. Sci. Lett., 74, 137–148.

Ghali, S., 2008. Introduction to Geometric Computing. Springer, London.

Gephart, J.W., Forsyth, D.W., 1984. An improved method for determining the regional stress tensor using earthquake focal mechanism data: application to the San Fernando earthquake sequence. J. Geophys. Res. 89, 9305–9320.

Gómez, J.L.S., 1986. Analysis of a gradual change in stress regime (example from the Eastern Iberian Chain, Spain). Tectonophysics 124, 37–53.

Groshong, R.H., 1972. Strain calculated from twinning in calcite. Geol. Soc. Am. Bull., 83, 2025–2038.

Gushchenko, O.I., 1973.. Analysis of the orientations of the slip on the fault plane and their tectonophysical interpretation during the reconstruction of palaeostresses. Doklady Akademii Nauk SSSR 210, 331–334.

Hyndman, R.D., Weichert, D.H., 1983. Seismicity and rates of relative motion on the plate boundaries of Western North America. Geophys. J. Roy. Astr. Soc. 72, 59–82.

Il'yushin, A.A., 1954. On a connection between stresses and small strains in the mechanics of continuous media. Prikl. Mat. Mekh. 18, 641–666 (in Russian).

Il'yushin, A.A., 1961. On the postulate of plasticity. Prikl. Mat. Mekh. 25, 503–507 (in Russian).

Jackson, J., McKenzie, D., 1988. The relationship between plate motions and seismic moment tensors, and the rates of active deformation in the Mediterranean and Middle East. Geophys. J. Int. 93, 45–73.

Kassaras, I.G., Kapentanidis, V., 2018. Resolving the tectonic stress by the inversion of earthquake focal mechanisms. Application in the region of Greece. A tutorial. In, D'Amico, S. (ed.), Moment Tensor Solutions: A Useful Tool for Seismotectonics, Springer, Cham, 405–452.

Khan, A.S., Huang, S., 1995. Continuum Theory of Plasticity. John Wiley & Sons, New York.

Kocks, U.F., Tomé, C.N., Wenk, H.-R., 1998. Texture and Anisotropy: Preferred Orientations in Polycrystals and Their Effects on Materials Properties. Cambridge Univ. Press, Cambrdge.

Kostrov, B.V., 1974. Seismic moment and energy of earthquakes, and seismic flow of rocks. Izv. Acad. Sci. USSR Phys. Solid Earth 1, 23–44.

Lacombe, O., 2010. Calcite twins, a tool for tectonic studies in thrust belts and stable orogenic foreland. Oil Gas Sci. 65, 809–838.

Lacombe, O., 2012. Do fault slip data inversions actually yield "paleostresses" that can be compared with contemporary stresses? A critical discussion. Comp. Rend. Geosci. 344, 159–173.

Landau, L.D., Lifshitz, E.M., 1976. Mechanics, 3rd Ed. Butterworth-Heinemann, Oxford.

Lejri, M., Maerten, F., Maerten L., Soliva R., 2015. Paleostress inversion: A multi-parametric geomechanical evaluation of the Wallace-Bott assumptions. Tectonophysics 657, 129–143.

Lejri, M., Maerten, F., Maerten L., Soliva R., 2017. Accuracy evaluation of both Wallace-Bott and BEM-based paleostress inversion methods. Tectonophysics 694, 130–145.

Lipschutz, S., Spellman, D., Spiegel, M.R., 2009. Schaum's Outline of Vector Analysis, 2nd Ed. McGraw-Hill, New York.

Lisle, R.J., 1987. Principal stress orientations from faults: an additional constraint. Ann. Tectonicae 1, 155–158.

Lisle, R.J., 2013. A critical look at the Wallace-Bott hypothesis in fault-slip analysis. Bull. Soc. Géol. Fr. 184, 299–306.

Lisle, R.J., Orife, T.O., Arlegui, L., 2001. A stress inversion method requiring only fault slip sense. J. Geophys. Res. 106, 2281–2289, doi:10.1029/2000JB900353.

Malvern, L.E., 1969. Introduction to the Mechanics of a Continuous Media. Prentice-Hall, Englewood Cliffs.

Marrett, R., Allmendinger, R.W., 1990. Kinematic analysis of fault-slip data. J. Struct. Geol. 12, 973–986.

Matsumoto, S., 2016. Method for estimating the stress field from seismic moment tensor data based on the flow rule in plasticity theory. Geophys. Res. Lett. 43, 8928–8935.

Mattauer, M., 1973. Les Déformations des Matériaux de L'Écorce Terrestre. Hermann, Paris.

Maury, J., Cornet, F.H., Dorbath, L., 2013. Access denied A review of methods

for determining stress fields from earthquakes focal mechanisms; Application to the Sierentz 1980 seismic crisis (Upper Rhine graben). Bull. Soc. Geol. Fr. 184, 319–334.

McFarland J.M., Morris, A.P., Ferrill, D.A., 2012. Stress inversion using slip tendency. Comp. Geosci. 41, 40–46.

Meyer, C., 2000. Matrix Analysis and Applied Linear Algebra. SIAM, Philadelphia.

Michael, A.J., 1987. Use of focal mechanisms to determine stress: a control study. J. Geophys. Res. 92, 357-368.

Molnar, P., 1983. Average regional strain due to slip on numerous faults of different orientation. J. Geophys. Res. 88, 6430–6432.

Morris, A., Ferrill, D.A., Henderson, D.B., 1996. Slip-tendency analysis and fault reactivation. Geology 24, 275–278.

Nemcock, M., Kovác, D., Lisle, R.J., 1999. A stress inversion procedure for polyphase calcite twin and fault/slip data sets. J. Struct. Geol. 21, 597–611.

Nemcok, M., Lisle, R.J., 1995. A stress inversion procedure for polyphase fault/slip data sets. J. Struct. Geol. 17, 1445–1453.

Nieto-Samaniego, A.F., Alaniz-Alvarez, S.A., 1997. Origin and tectonic interpretation of multiple fault patterns. Tectonophysics 270, 197–206.

Orife, T. and Lisle, R.J., 2003. Numerical processing of paleostress results. J. Struct. Geol. 25, 949–957.

Otsubo, M., Yamaji, A., 2006. Improved resolution of the multiple inverse method by eliminating erroneous solutions. Comp. Geosci. 32, 1221–1227.

Otsubo, M., Yamaji, A., Kubo, A., 2008. Determination of stresses from heterogeneous focal mechanism data: An adaptation of the multiple inverse method. Tectonophysics 457, 150–160

Ottosen, N.S., Ristinmaa, M., 2005. The Mechanics of Constitutive Modeling. Elsevier, Amsterdam.

Payne, H., 1959. The slip theory of plasticity for crystalline aggregates. J. Mech. Phys. Solids 7, 126–134.

Parlangeau, C., Lacombe, O., Schueller, S., Daniel, J.-M., 2018. Inversion of calcite twin data for paleostress orientations and magnitudes: A new technique tested and calibrated on numerically-generated and natural data Tectonophysics 722, 462–485.

Pascal, C., 2002. Interaction of faults and perturbation of slip: Influence of anisotropic stress states in the presence of fault friction and comparison between Wallace-Bott and 3D distinct element models. Tectonophysics 356, 307–322.

Petit, J.P., 1987. Criteria for the sense of movement on fault surfaces in brittle rocks. J. Struct. Geol. 9, 597–608.

Pollard, D.D., Saltzer, S.D., Rubin, A.M., 1993. Stress inversion methods: are they based on faulty assumptions? J. Struct. Geol. 15, 1045–1054.

Prager, W., 1949. Recent developments in the mathematical theory of plasticity. J. Appl. Phys. 20, 235–241.

Ramsay, J.G., Lisle, R., 2000. The Techniques of Modern Structural Geology, Volume 3: Applications of Continuum Mechanics in Structural Geology. Academic Press, San Diego.

Rebetsky, Yu.L., 1997. Reconstruction of tectonic stresses and seismotectonic strains: Methodical fundametnals, current stress field of southeastern Asia and Oceania. Doklady Earth Sci. 354, 560–563.

Rebetsky, Yu.L., 1999. Methods for reconstructing tectonic stresses and seismotectonic deformations based on the modern theory of plasticity. Doklady Earth Sci. 365A, 370–373.

Rebetsky, Yu.L., Kuchai, O.A., Sycheva, N.A., Tatevossian, R.E., 2012. Development of inversion methods on fault slip data: Stress state in orogenes of the Central Asia. Tectonophysics 581, 114–131.

Rocher, M., Cushing, M., Lemeille, F., Lozac'h, Y., Angelier, J., 2004. Intraplate paleostresses reconstructed with calcite twinning and faulting: Improved method and application to the eastern Paris Basin (Lorraine, France). Tectonophysics 387, 1–21.

Sato, K., 2006. Incorporation of incomplete fault-slip data into stress tensor inversion. Tectonophysics 421, 319–330.

Sato, K., 2012a. Fast multiple inversion for stress analysis from fault-slip data. Comp. Geosci. 40, 132–137.

Sato, K., 2012b. Physical meaning of Stress difference for fault-slip analysis. Math. Geosci. 44, 635–644.

Sato, K., 2012c. Fast multiple inversion for stress analysis from fault-slip data. Comp. Geosci. 40, 132–137.

Sato, K., 2016. A computerized method to estimate friction coefficient from orientation distribution of meso-scale faults. J. Struct. Geol. 89, 44–53.

Sato, K., Yamaji, A., 2006a. Embedding stress difference in parameter space for stress tensor inversion. J. Struct. Geol. 28, 957–971.

Sato, K., Yamaji, A., 2006b. Uniform distribution of points on a hypersphere for improving the resolution of stress tensor inversion. J. Struct. Geol. 28, 972–979.

Shan, Y., Lin, G., Li, Z., 2004a. An inverse method to determine the optimal stress from imperfect fault data. Tectonophysics 387, 1–4.

Shan, Y., Li, Z., Lin, G., 2004b. A stress inversion procedure for automatic recognition of polyphase fault/slip data sets. J. Struct. Geol. 26, 919–925.

Shan, Y., Suen, H., Lin, G., 2003. Separation of polyphase fault/slip data: an objective-function algorithm based on hard division. J. Struct. Geol. 25, 829–840.

Shan, Y., Zheng, J., Liang, X., 2019. Synthetic slip plane, the combination of a pair of twinned and untwinned e-planes in a single calcite crystal: Application in dynamic analysis. J. Struct. Geol. 119, 81–92. Calculus and Analysis in Euclidean Space

Shurman, J., 2016. Calculus and Analysis in Euclidean Space. Springer, Cham.

Stephens, T.L., Walker, R.J., Healy, D., Bubeck, A., England, R.W., 2018. Mechanical models to estimate the paleostress state from igneous intrusions. Solid Earth 9, 847–858.

Tavani, S., Storti, F., Lacombe, O., Corradetti, A., Muñoz, J.A., Mazzoli, S., 2015. A review of deformation pattern templates in foreland basin systems and fold-and-thrust belts: Implications for the state of stress in the frontal regions of thrust wedges. Earth Sci. Rev. 141, 82–104.

Tikoff, B., Blenkinsop, T., Kruckenberg, S.C., Morgan, S., Newman, J., Wojtal, S., 2013. A perspective on the emergence of modern structural geology: Celebrating the feedbacks between historical-based and process-based approaches. Spec. Publ. 500, Geol. Soc. Am., 65–119.

Tonai, S., Sato, K., Ashi, J., 2011. Incremental fold test for paleostress analysis using the Hough transform inverse method. J. Struct. Geol. 33, 1158–1168.

Tranos, M.D., 2015. TR method (TRM): A separation and stress inversion method for heterogeneous fault-slip data driven by Andersonian extensional and compressional stress regimes. J. Struct. Geol. 79, 57–74.

Turner, F.J., 1953. Nature and dynamic interpretation of deformation lamellae in calcite of three marbles. Am. J. Sci. 251, 276–298.

Tsutsumi, H., Sato, K., Yamaji, A., 2012. Stability of the regional stress field in central Japan during the late Quaternary inferred from the stress inversion of the active fault data. Geophys. Res. Lett. 39, L23303, doi:10.1029/2012GL054094.

Wallace, R. E., 1951. Geometry of shearing stress and relationship to faulting. Journal of Geology 59, 111–130.

Wu, H.-C., 2005. Continuum Mechanics and Plasticity. Capman & Hall, Boca Raton.

Yamaji, A., 2000. The multiple inverse method: a new technique to separate stresses from heterogeneous fault-slip data. J. Struct. Geol. 22, 441–452.

Yamaji, A., 2003. Are the solutions of stress inversion correct? Visualization of their reliability and the separation of stresses from heterogeneous fault-slip data. J. Struct. Geol. 25, 241–252.

Yamaji, A., 2013. Two-dimensional finite deformations evaluated from pre- and post-deformation markers: Application to balanced cross sections. J. Struct. Geol. 51, 144–155.

Yamaji, A., 2015a. How tightly does calcite e-twin constrain stress? J. Struct. Geol. 72, 83–95.

Yamaji, A., 2015b. Generalized Hough transform for the stress inversion of calcite twin data. J. Struct. Geol. 80, 2–15.

Yamaji, A., Otsubo, M., Sato, K., 2006. Paleostress analysis using the Hough transform for separating stresses from heterogeneous fault-slip data. J. Struct. Geol. 28, 980–990.

Yamaji, A., Sato, K., 2006. Distances for the solutions of stress tensor inversion in relation to misfit angles that accompany the solutions. Geophys. J. Int. 167, 933–942.

Yamaji, A., Sato, K., 2011. Clustering of fracture orientations using a mixed Bingham distribution and its application to paleostress analysis from dike or vein orientations. J. Struct. Geol. 33, 1148–1157.

Yamaji, A., Tomita, S., Otsubo, M., 2005. Bedding tilt test for paleostress analysis. J. Struct. Geol. 27, 161–170.

Žalohar, J., Vrabec, M., 2007. Paleostress analysis of heterogeneous fault-slip data: The Gauss method. J. Struct. Geol. 29, 1798–1810.

Table 1: List of symbols.

Symbols	Explanations
$\boldsymbol{b}$	unit vector perpendicular to $\boldsymbol{n}$ and $\boldsymbol{v}$
D_{M}	Michael distance
D_{OM}	Orife-Lisle distance
great circle $[n]$	the intersection of an hyperplane $[n]$ and higher dimensional sphere
$\vec{h}$	5D unit vector corresponding to $\boldsymbol{\varepsilon}$
hyperplane $[n]$	nD subspace in a higher dimensional space
$\boldsymbol{n}$	unit normal vector
$\vec{P}$	6D vector
$\vec{p}$	5D unit vector corresponding to $\boldsymbol{\varepsilon}'$
$P(\ )$	probability density function
$\boldsymbol{Q}$	3D orthogonal matrix representing principal axes
$\boldsymbol{R}$	3D or 6D rotation matrix
$\vec{s}$	5D unit vector representing reduced stress tensor
$\mathrm{S}_5, \mathrm{S}_6$	5D and 6D unit hypersphere
$\boldsymbol{v}$	unit vector indicating the slip direction of footwall
$\boldsymbol{X}$	3D, symmetric, deviatoric tensor
$\vec{X}$	6D vector corresponding to $\boldsymbol{X}$
X_{II}	the second basic invariant of $\boldsymbol{X}$
$\vec{Y}$	5D vector corresponding to $\boldsymbol{X}$
$\Delta\sigma$	differential stress
$\boldsymbol{\epsilon}$	reduced strain tensor representing $\boldsymbol{n}$ and $\boldsymbol{v}$
$\boldsymbol{\epsilon}'$	reduced strain tensor representing $\boldsymbol{n}$ and $\boldsymbol{b}$
$\vec{\epsilon}$	6D unit vector corresponding to $\boldsymbol{\varepsilon}$
$\vec{\epsilon}'$	6D unit vector corresponding to $\boldsymbol{\varepsilon}'$
Θ	angular stress distance
κ_1, κ_2	concentration parameters
Λ	Lode angle
λ	axiality
σ	stress tensor or deviatoric stress tensor
$\underline{\sigma}$	non-dimensional deviatoric stress tensor
$\underline{\varsigma}$	reduced stress tensor
$\vec{\varsigma}$	6D vector corresponding to ς
$\sigma_1, \sigma_2, \sigma_3$	principal stresses
τ	shear stress
τ_{c}	critical resolved shear stress
Φ	stress ratio, shape ratio
Ψ	radius of a spherical cap on S_5

Table 2: Dissimilarity classes of reduced stress tensors adjusted to practical stress inversion studies. A parenthesis and a square bracket denote the open and closed endpoints of an interval, respectively. Stresses with $\Theta = 0$ and $180°$ are equivalent and opposite stresses, respectively.

	Θ	D_{OL}
very similar	(0.00°, 28.09°)	(0.000, 0.485)
similar	[28.09°, 43.17°)	[0.485, 0.736)
resemble	[43.17°, 59.26°)	[0.736, 0.989)
different	[59.26°, 136.83°)	[0.989, 1.729)
very different	[136.83°, 180.00°)	[1.729, 2.00)